CHALMERS

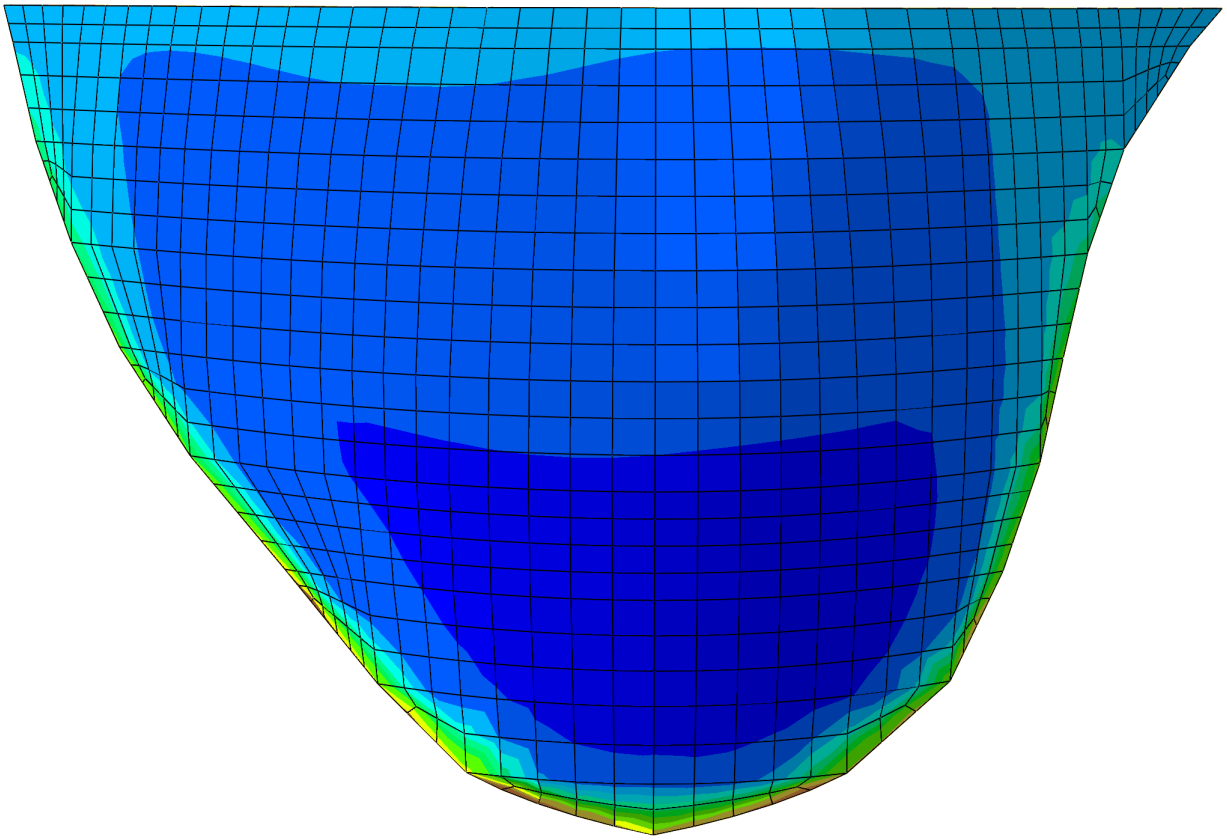

Stability analysis of the hydropower arch dam Jinping I in China

Master of Science Thesis in Applied Physics

Rebecka Johansson & Emma Kronberg

Department of Applied Physics
Chalmers University of Technology
Göteborg, Sweden 2011

Cover:
Maximal principal stress on the upstream dam face for normal water level and maximum temperature.

THESIS FOR THE DEGREE OF MASTER OF SCIENCE

Stability analysis of the hydropower arch dam Jinping I in China

Rebecka Johansson & Emma Kronberg

CHALMERS

Department of Applied Physics
Chalmers University of Technology
Göteborg, Sweden 2011

Abstract

To meet the increasing demand of electric power in China, several hydropower plants are planned to be constructed the coming years. One of these is Jinping I, which will include the worlds tallest arch dam. It will be constructed at the Yalong river in Sichuan province and will be in operation by the year 2015. The purpose of this master's thesis is to evaluate the stability of the Jinping I dam under static and dynamic conditions. Stresses in the dam were calculated using linear finite element method. The stability of the dam was evaluated through comparison of the calculated stresses with both the strength of concrete and to stresses acquired through similar FEM-analyses of another Chinese arch dam, the Ertan dam.

Under static conditions, problematic stresses were tensile stresses that exceeded the strength of concrete, these occurred under specific conditions and in limited areas which were situated so that they are easily accessed in case of restoration. Overall, the calculated stresses showed that the dam is able to withstand both normal and extreme static load cases without severe damage. In the dynamic case it was more relevant to compare with the Ertan dam since stresses exceeding the strength of concrete and damages of the dam are allowed. The stresses of the Jinping I dam were similar to stresses of the Ertan dam and were thus concluded to be acceptable for an earthquake of this probability.

Sammanfattning

För att möta den stigande efterfrågan av elektricitet i Kina finns planer för att bygga flera vattenkraftverk i landet. Ett av kraftverken är Jinping I som kommer att inkludera världens högsta valvdamm. Dammen kommer byggas i Yalongfloden i Sichuanprovinsen och beräknas vara i drift 2015. Syftet med denna masteruppsats är att undersöka stabiliteten av Jinping I-dammen under statiska och dynamiska förhållanden. Spänningarna i dammen beräknades med linjära finita elementmetoden. Stabiliteten av dammen bedömdes genom att jämföra de beräknade spänningarna både med hållfastheten av betong och spänningarna från en liknande FEM-analys av en annan kinesisk valvdamm, Ertandammen.

Under statiska förhållanden, var de problematiska spänningarna dragspänningarna som översteg hållfastheten för betong, dessa spänningar förekommer under specifika förhållanden och i begränsade delar av dammen vilka är lättåtkomliga vid en eventuell restaurering. De beräknade spänningarna visade att dammen är kapabel att klara av både normala och extrema statiska krafter utan att skadas allvarligt. I det dynamiska fallet var det mer relevant att jämföra med Ertandammen eftersom spänningar som överstiger hållfastheten för betong och skador på dammen är tillåtna. Spänningarna på Jinping I-dammen motsvarar spänningarna på Ertan dammen och kan därför ses som acceptabla för en jordbävning av denna sannolikhet.

Acknowledgement

The project reported in this Master degree thesis has been carried out at Department of Hydraulic Engineering at Tsinghua University, Beijing, from March to June 2011.

We are grateful to our supervisor Prof. Jin Feng for inviting us to Tsinghua University and for the advices and interesting discussions. We would also like to devote our thanks to Gui Yao at the university for all the help offered to us during our stay.

We owe our thanks to Dr. James Yang from Vattenfall R&D/KTH for making the trip possible and for all necessary arrangements and to Prof. Göran Wahnström, our examiner at Chalmers Tekniska Högskola, for all the help.

This project is funded by Elforsk AB within the frame of dam safety, where Mr. Cristian Andersson and Mrs. Sara Sandberg are program directors. Some funding is also obtained from Chalmers Tekniska Högskola which facilitates the accomplishment of the project.

Göteborg, August 2011

Rebecka Johansson & Emma Kronberg

Contents

Abbreviations

DOF	Degree of freedom
FEM	Finite element method

Symbols

a_0,a_1	Damping factors
c	Viscous damping coefficient
E	Elastic modulus
ϵ	Strain
f_I	Inertia force
f_D	Damping force
f_S	Elastic force
G	Shear modulus
γ	Shear strain
k	Stiffness
m	Mass
ν	Poissons ratio
ω	Frequency
p	External force
σ	Stress
T_d	Temperature difference
T_m	Mean temperature
τ	Shear stress
u	Displacement
$\dot{u}$	Velocity
$\ddot{u}$	Acceleration
ξ	Damping ratio

Chapter 1:

Introduction

The demand for electric power in China is growing each year and the power system is continuously expanded. For the time being, coal combustion contributes with the majority of the power produced, with large emissions of CO_2 and smoke pollution as a consequence. Hydropower is the second largest source of electric power, however, in the year 2007 it only accounted for 15 % of the total energy generated. To meet the increasing demand of electric power China is planning to develop its hydropower resources, almost doubling the installed capacity. This effort includes, among other projects, the Three Gorges Project, which will have the largest installed capacity in the world, and the Jinping Project, consisting of a sluice dam and the worlds highest arch dam, Jinping I.

Jinping I is planned to be in operation in 2015 and is designed to have a capacity of 3 600 MW and an annual power output of 16.6 TWh. The dam will be 305 m high and have a water head of 240 m. An arch dam of this size is subjected to huge forces that it has to resist in order to avoid damage. A hydropower plant is a project demanding large investments and involves big risks to surrounding eco-systems, structures and human lives. The long-term stability of the dam structure is thus of great importance to avoid economic loss and loss of human lives.

1.1 Purpose

The main purpose of this master thesis is to evaluate the stability of the Jinping I concrete arch dam under static and dynamic conditions using the finite element method.

1.2 Limitations

The most important limitation in this thesis was the use of linear analysis, since the more accurate non-linear analysis would be more time-consuming and not suited for a thesis of this size. Also, only the stresses in the dam were considered in the stability analysis, while the stresses in the foundation were beyond the scope of this thesis.

1.3 Method

The stability analysis was based on stress calculations on critical parts of the dam. The stress analysis of the dam was performed in Abaqus, a software based on finite element analysis. In the static analysis the dam structure was studied independently of time or load history. Loads included in this analysis were: hydrostatic, self-weight, sediment, and temperature load. Six different load cases were evaluated, considering different water and temperature conditions. The maximal and minimal principal stresses were evaluated at the

upstream and downstream faces of the dam.

In the dynamic analysis, time-dependent accelerations were applied to the model, to simulate an earthquake, in addition to the static loads. Maximal and minimal principal stresses were evaluated at the upstream and downstream dam faces. For each node the maximum value of the maximal principal stress and the minimum value of the minimal principal stress over the whole time span were evaluated. The stability of the dam, under static and dynamic conditions, was evaluated by comparing the stresses of the Jinping I dam with the strength of concrete, but also with stresses acquired under similar loads in another Chinese arch dam.

Chapter 2:

Background

2.1 Energy situation in China

As a developing country, China's use of and dependence on electric power has increased greatly the last decades. From 1978 to 2008 the installed capacity grew from 57 GW to 793 GW [1]. The development of installed capacity can be seen in figure 2.1. Between 2003 and 2008, the installed capacity more than doubled and the total power output in 2007 reached 3 256 TWh, only second to the United States that reached 4 157 TWh.

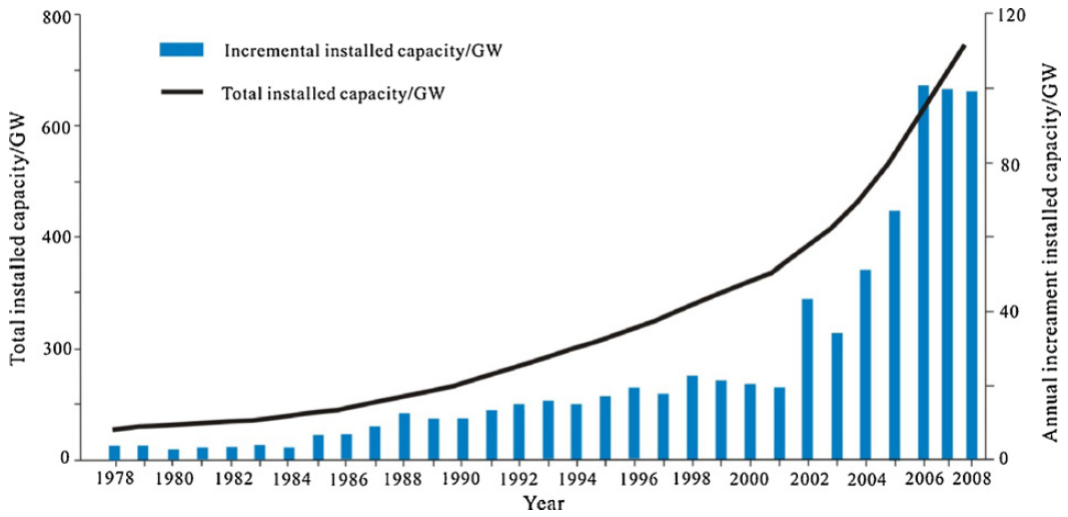

Figure 2.1: *Total installed capacity and annual increment in installed capacity [1].*

Expansion of the power system has mainly been driven by industrial growth. In 1980, during the early years of economic reform, roughly 80 % of China's produced electricity was consumed by industry. The residential and commercial demand increased rapidly in quantity over the 1990s and 2000s. In 2007 the residential and commercial consumption reached 626 TWh. The total consumption in 1990 was 580 TWh, while the industrial consumption still constitutes 70 % of China's electricity demand [2].

Coal accounts for the majority of both the installed capacity and the power generated, see figure 2.2. In 2007 83 % of the power generated originated from coal, far greater than the world average of 40 %. The consumption of coal is not only a source of electric power but also a cause for large emissions of greenhouse gases. Coal combustion accounted for 82 % of China's CO_2 emissions in 2006 and is the main cause of smoke pollution in the country. Ex-

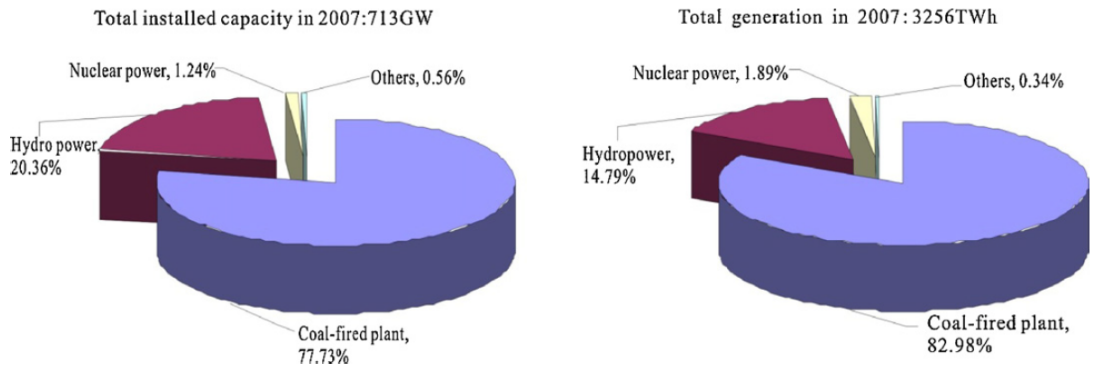

Figure 2.2: *Allocation of electric power generation according to type of source in the year 2007 [1].*

cessive coal production is a cause for almost constant acid rain in a third of China's territory.

The second largest source of electric power in China is hydropower. In 2007 the installed capacity and energy generation of hydropower reached 145.26 GW and 486.7 TWh accounting for 15 % of the total energy generated.

The third largest source for electric power generation is nuclear power. Nuclear power has a relatively short history in China, the first power plant went into operation in 1991 and by 2007 China had 11 units with an installed capacity of 8.6 GW providing 62.86 TWh. China has its own resources of uranium in low-grade ores. Domestic sources supply around half of the needs, the rest is imported. China's insufficient reserves of natural uranium and the lack of highly trained professionals in the field are the main barriers to the development of nuclear energy. Also, spent fuel management is a politically sensitive topic that has not been adressed in the same extent as the construction of new nuclear power plants.

Other sources for power generation are, among others, wind power, solar energy, and biomass energy. The development of renewable power sources is held back for different reasons. Wind power is relatively cheap but decreases the accuracy of power generation forecast and impacts the stability of the power grid. The increasing price of crop stalks has made biomass a less attractive power source while the most prominent barrier to development of solar power is the cost. Hydropower is the cheapest power source, followed by coal combustion. Although, the development of hydropower has its own restrictive factors, explained below.

2.1.1 Hydropower in China

China has a large quantity of rivers, more than 50 000 of which 3 886 have a hydropower potential over 10 MW. The theoretical hydropower potential and annual average energy generation of mainland China are estimated as 694 GW and 6 080 TWh/year [3]. The technically exploitable installed capacity and annual average energy generation have been estimated to 542 GW and 2 470 TWh/year while the economically exploitable ones have been estimated as 402 GW and 1 750 TWh/year. The most fruitful hydropower resources are situated in four provinces in Southwest China; Sichuan, Yunnan, Tibet and Guizhou.

The first hydropower station in China was built in 1912 in Shilongba, Yunnan Province with an installed capacity of 500 kW. Since the establishment of the People's Republic of China in 1949 hydropower has developed rapidly with installed capacity and energy genera-

tion growing with a rate of 12.4 % and 11.9 % annually. In 2005 both the installed capacity and the energy generation of Chinese hydropower were ranked first in the world and China had a 13.3 % share of the world's total hydropower production, even though hydropower only accounts for a minor share of China's total electricity production.

China is planning to develop electric generation in 13 hydropower bases distributed among the hydropower resources. If the resources are completely developed in these bases the installed capacity of hydropower will reach 275.77 GW. Several of the planned hydropower projects are world-class projects. Examples include the Three Gorges Project that is planned to have the largest installed capacity in the world, the Jinping I Hydropower Project to have the highest arch dam of 305 m and Shuibuya Hydropower Project to have the highest face rockfill dam of 233 m.

Hydropower is a clean and renewable energy source with high efficiency compared to other energy sources, modern hydropower turbines are able to convert 90 % of available energy into electricity, while the same number for the best fossil fuel plants is around 50 %. The potential energy of high water is used to generate electricity and therefore the only fuel required is water which is not depleted in the process. An advantage of hydropower is that the power output can be changed quickly to meet any changes in demand. In addition, hydropower does not create any toxic by-products and does not produce air pollutants.

Although there are many advantages using hydropower compared to other sources for generating electricity there are some drawbacks and restrictive factors related to it. The temporal and spatial distribution of precipitation in China is very uneven, leading to large variations in river flow between flood and dry season and between wet and dry years. The solution is to use reservoirs to regulate the water flow. The storage capacity of the reservoirs need to be very huge leading to large investments and resettlement of local population. The distribution of hydropower resources is presented in figure 2.3, due to larger precipitation in the western parts of the country the hydropower facilities are concentrated there, requiring long-distance transmission to the east. Long-distance transmission of electricity is both expensive and involves losses. The construction of hydropower plants and reservoirs inevitably leads to flooding of surrounding areas. Changes in the environment requires resettlement and negatively impacts the ecosystem. While operated, some of the hydropower plants give priority to flood protection and irrigation, while the majority have energy generation as their main purpose.

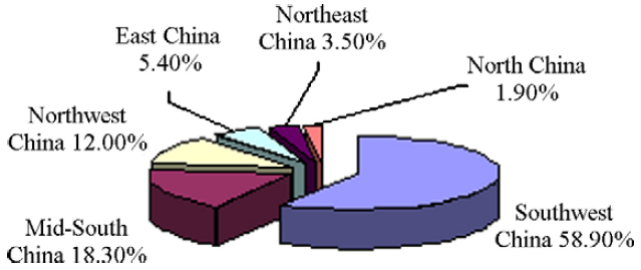

Figure 2.3: *Distribution of hydropower resources in China [3].*

2.2 The Jinping project

2.2.1 Yalong River

Jinping hydropower project is located at Great Jinping River Bend in the Yalong River [4]. The river is a tributary of the Yangtze river and located in Sichuan province in southwestern China. It is 1 571 km long and has a head, difference in height, of 3 830 m. Due to the high head and an average annual water flow of 1 910 m^3/s Yalong River has a great potential for hydropower. This has resulted in an arrangement scheme of 21 hydropower stations along the river. Together they will have a total capacity of 30 GW with an annual power generation of 150 TWh. The large power generation potential makes Yalong River the third largest hydropower base in China, after the Yangtze River and the Jinsha River.

2.2.2 Jinping

The Jinping project is expected to start operating in 2015 [4]. The hydropower station includes two different dams, Jinping I and Jinping II. Jinping I is an arch dam located upstream of the Great Jinping River Bend and Jinping II is a sluice dam located 7.5 km downstream from Jinping I.

The Jinping hydropower project will have a rated total capacity of 8 400 MW and generate 40.8 TWh annually. Around 70% of the generated electricity will be transmitted to developed areas in eastern China and the remaining part to Sichuan and Chongqing. In addition to power generation the Jinping project will control flooding for the middle and downstream sections of the Yangtze River [5]. The estimated cost is 54.4 billion Yuan or around 8 billion US$.

The location of the project provides an environment with deep valleys, rapid flow, no navigation, scarce population, little farm land and no big cities - favorable characteristics for a great hydropower base. Furthermore, 7 000 people have to be resettled to accomplish the project, a relatively small number for such a large project.

The geographic location of Jinping has the seismic intensity VII. Due to the seismic intensity a peak acceleration of 0.1 g have been considered in the design of the project.

2.2.3 Jinping I

The reservoir of Jinping I will range from Kala to Jiangkou [5]. The total reservoir volume will be 7.76 Gm^3 [4]. Jinping I is designed to have a capacity of 3 600 MW and an annual power output of 16.6 TWh. The main components of the hydropower station will be the arch dam, the power generation complex, the flood release structures and the diversion tunnels. A layout of Jinping I from above is shown in figure 2.4.

Jinping I will have a concrete double-curvature thin arch dam. A computer simulated picture of the dam can be seen in figure 2.5. The dam will be 305 m high, enabling a water head of 240 m. The width of the dam changes in vertical direction, however at the crest the arch is 552 m long. A cross-section of the dam is shown in figure 2.6 and a variation of the thickness can be observed. At the base the thickness is 63 m and at the crest 16 m. Further, the normal and the dead water level, the level at which the water leaves the basin for the turbines, are displayed in the figure, which are 1 880 m and 1 800 m above sea level.

The power generation complex will be located at the right bank of the river, see figure

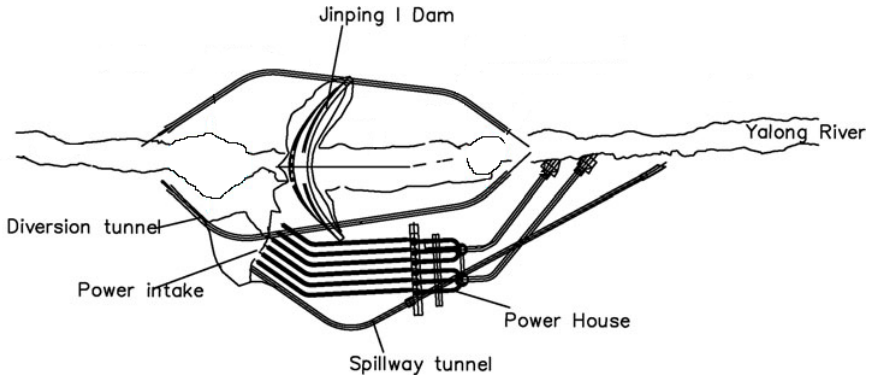

Figure 2.4: *The layout of Jinping I, seen from above [4].*

Figure 2.5: *Computer simulation of Jinping I [4].*

2.4. From the power intake the water is transported through penstocks to the six Francis turbines, each with a rated capacity of 600 MW, where the kinetic energy is converted to electricity. The purpose of the flood release structure is to control the water level in the reservoir by leading water safely from the reservoir to the downstream river [6]. In Jinping I four surface spillways and five lower level outlets will be included in the system, which can be seen in figure 2.6. Furthermore, the hydropower station will include a spillway tunnel on the right bank showed in figure 2.4. Diversion tunnels are used to lead the water around the structure. In figure 2.4 the two diversion tunnels are shown, one on each side of the river. The V-shaped canyon at Jinping I is shown in figure 2.7. The steep and high slopes, will result in high geological stress under natural conditions. For instance a major principal stress above 40 MPa has been measured at the toe of the slope. The deep valley implicates some technical challenges and the high geological stresses of Jinping I are currently considered the most difficult stability problems of all hydropower projects in China.

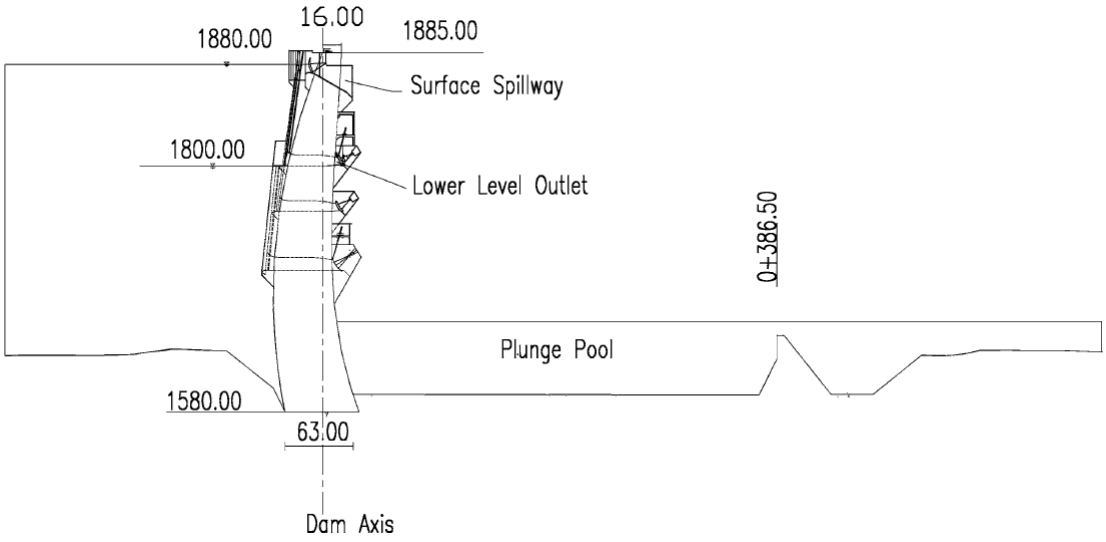

Figure 2.6: *Cross-section of the arch dam in Jinping I [4].*

Figure 2.7: *The canyon at the location of Jinping I [4].*

Chapter 3:

Theoretical background

3.1 Stress and strain

Stress and strain are introduced in a material when it is subjected to forces [7]. The stress, σ, is the internal force defined as force per cross-section unit and can be expressed as

$$\sigma = \frac{F}{\Omega} \tag{3.1.1}$$

where F is the applied force and Ω the cross-section. The material strength is determined by how much stress the material can withstand without failing. The strain, ϵ, describes the displacement between two points in a material. This corresponds to the deformation and is defined as

$$\epsilon = \frac{\Delta l}{l} \tag{3.1.2}$$

where Δl is the elongation and l is the original length of the material.

3.1.1 Stress-strain relations

The relation between stress and strain in elastic materials can be described by the stress-strain diagram in figure 3.1 [7]. The arrows emphasise that the stress-strain relation follows the same curve under loading and unloading which is a property of elastic materials. Furthermore, the final strain in the material after loading is not affected by the history of loading, which means that the final strain is independent by the path to reach point 1 in figure 3.1. Another property of elastic materials is that the curve is time-independent, so the loading rate is not important as long as it does not cause any dynamic effects. As illustrated in figure 3.1, there is a linear relation between stress and strain in small stresses, and a linear approximation of the stress-strain relation is frequently used to describe structural materials. In the linear stress-strain diagram in figure 3.2, the curve is described by Hooke's law

$$\sigma = E\epsilon \tag{3.1.3}$$

where E is Young's modulus. For non-linear elastic material, the curve in the stress-strain diagram indicates that the relation is not linear and can not be described with the linear Hooke's law. However, by defining a tangent elasticity modulus, E_t, the curvature can be described. The expression of the tangent elasticity modulus is

$$E_t = \frac{d\sigma}{d\epsilon} \tag{3.1.4}$$

where $d\sigma$ and $d\epsilon$ correspond to the change in stress and strain due to the applied force.

In elastic-plastic materials the stress-strain relation does not follow the same curve for

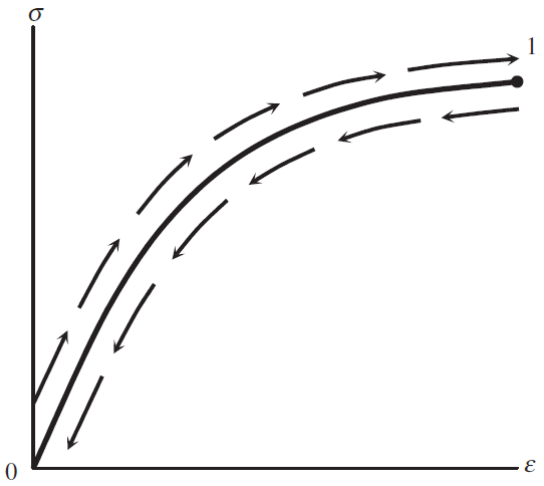

Figure 3.1: *Non-linear elastic stress-strain curve [7].*

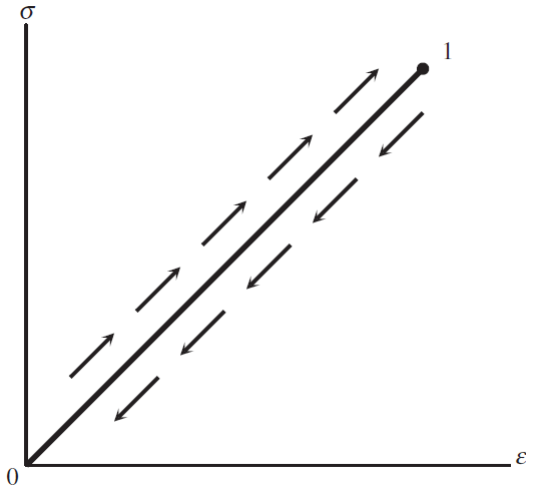

Figure 3.2: *Linear elastic stress-strain curve [7].*

loading and unloading, which can be seen in figure 3.3. The elastic strain, ϵ_e, goes to zero while the plastic strain, ϵ_p, remains in the material after unloading. Like elastic materials the stress-strain relation in elastic-plastic materials is time-independent, on the other hand they depend on the history of loading.

Even though the stress-strain relation for both elastic and elastic-plastic materials are time-independent, the relation can become time-dependent under certain temperature conditions. The temperature when the relation becomes time-dependent depends on the material's properties. However, a relatively high temperature is required for most materials. The time-dependent strain induced in a material under a constant force due to temperature is called the creep of the material. The creep strain, ϵ_c, has both a reversible and a residual part. The final strain in a material is thus given as

$$\epsilon = \epsilon_e + \epsilon_p + \epsilon_c \tag{3.1.5}$$

In most practical applications it is assumed that the material is elastic or that the applied force does not induce enough strain to reach the plastic region, implying that $\epsilon_p \ll \epsilon_e$. Furthermore, it is assumed that either the material is not subjected to creep or that the

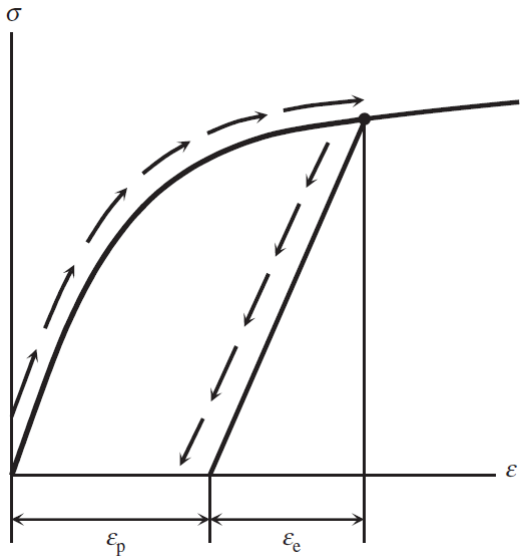

Figure 3.3: *Elastic-plastic stress-strain curve [7].*

load is applied in a short time period so that $\epsilon_c \ll \epsilon_e$. Therefore, the total strain can be approximated as the elastic strain, ϵ_e.

3.1.2 Ductile and brittle material behaviour

The relation between an axial force N applied to a material, and the corresponding elongation δl is a main characteristic of a material's rheological behaviour [8]. The relation is fundamentally different for different kinds of materials. For ductile materials the relation between force and elongation is divided into several zones where the relation has different properties. For smaller elongations, the relation is linear and elastic, while for larger elongation the material behaves plastic. Before rupture the cross-section of the specimen decreases, a phenomenon known as necking. For brittle materials such as cast iron, concrete, rock, etc., the force-elongation relation is shown schematically in figure 3.4. The slope of the curve decreases until rupture, and rupture occurs with little plastic deformation. Further, the behaviour under tensile and compressive forces differs. Brittle materials generally display more stiffness and strength under compressive loading.

3.1.3 Poisson's ratio

Generally, when a force is applied to a material an elongation in one direction results in a shortening in another direction [8]. The longitudinal and transversal elongation is determined by Poisson's ratio, ν, in the relationship

$$\epsilon_t = -\nu\epsilon_l \tag{3.1.6}$$

where ϵ_t and ϵ_l is the strain in transversal and longitudinal direction, respectively.

3.1.4 Hooke's law for shear stress

Hooke's law in equation (3.1.3) expresses the relation between stress and strain in a material. In the same manner, Hooke's law for shear stress defines the relation between the shear stress, τ and the shear strain, γ

$$\tau = G\gamma \tag{3.1.7}$$

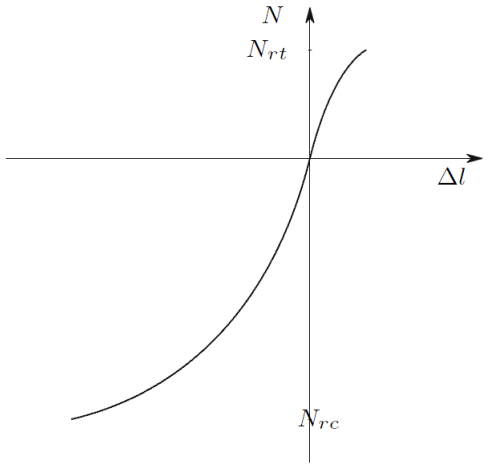

Figure 3.4: *Force-elongation relation for brittle materials, where N_{rt} and N_{rc} are the tensile and compressive rupture forces [8].*

where G is the shear modulus [9]. The shear strain is the angle caused by the shear stress shown in figure 3.5. The shear modulus is related to Young's modulus and Poisson's ratio according the expression

$$G = \frac{E}{2(1+\nu)} \tag{3.1.8}$$

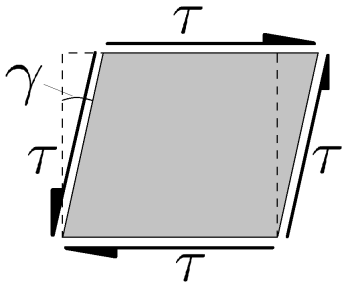

Figure 3.5: *Illustration of the shear strain, γ, caused by the shear stress, τ.*

3.1.5 Hooke's law in three dimensions for isotropic materials

Hooke's law, equation (3.1.3), in one direction is given as

$$\sigma_x = E\epsilon_x \tag{3.1.9}$$

where σ_x and ϵ_x correspond to stress and strain in the x-direction [9]. From the definition of Poisson's ratio and the property of isotropic materials that the reduction in $y-$ and $z-$direction are equal, the strain in y- and z-direction can be expressed as

$$\epsilon_y = \epsilon_z = -\nu\epsilon_x = -\nu\frac{\sigma_x}{E} \tag{3.1.10}$$

The linear relation between stress and strain implies that the superposition principle is valid. Addition of the stresses result in the following expression for linear elastic isotropic

materials,

$$\begin{aligned}\epsilon_x &= \frac{1}{E}(\sigma_x - \nu(\sigma_y + \sigma_z)) \\ \epsilon_y &= \frac{1}{E}(\sigma_y - \nu(\sigma_x + \sigma_z)) \\ \epsilon_z &= \frac{1}{E}(\sigma_z - \nu(\sigma_x + \sigma_y))\end{aligned} \tag{3.1.11}$$

In the same way Hooke's law for shear stress can be written in component form

$$\gamma_{xy} = \frac{\tau_{xy}}{G} \tag{3.1.12}$$

As with the stress-strain relation the shear stress-strain relation is linear, resulting in following expression for the shear strain,

$$\begin{aligned}\gamma_{xy} &= \tau_{xy}\frac{2(1+\nu)}{E} \\ \gamma_{yz} &= \tau_{yz}\frac{2(1+\nu)}{E} \\ \gamma_{zx} &= \tau_{zx}\frac{2(1+\nu)}{E}\end{aligned} \tag{3.1.13}$$

The equations in (3.1.11) and (3.1.13) can be written in matrix form

$$\begin{bmatrix}\epsilon_x \\ \epsilon_y \\ \epsilon_z \\ \gamma_{xy} \\ \gamma_{yz} \\ \gamma_{zy}\end{bmatrix} = \frac{1}{E}\begin{bmatrix}1 & -\nu & -\nu & 0 & 0 & 0 \\ -\nu & 1 & -\nu & 0 & 0 & 0 \\ -\nu & -\nu & 1 & 0 & 0 & 0 \\ 0 & 0 & 0 & 2(1+\nu) & 0 & 0 \\ 0 & 0 & 0 & 0 & 2(1+\nu) & 0 \\ 0 & 0 & 0 & 0 & 0 & 2(1+\nu)\end{bmatrix}\begin{bmatrix}\sigma_x \\ \sigma_y \\ \sigma_z \\ \tau_{xy} \\ \tau_{yz} \\ \tau_{zx}\end{bmatrix} \tag{3.1.14}$$

To obtain an expression for the stresses the inverse of the matrix in (3.1.14) is required, leading to the relation

$$\begin{bmatrix}\sigma_x \\ \sigma_y \\ \sigma_z \\ \tau_{xy} \\ \tau_{yz} \\ \tau_{zx}\end{bmatrix} = \underbrace{\frac{E}{(1+\nu)(1-2\nu)}\begin{bmatrix}1-\nu & \nu & \nu & 0 & 0 & 0 \\ \nu & 1-\nu & \nu & 0 & 0 & 0 \\ \nu & \nu & 1-\nu & 0 & 0 & 0 \\ 0 & 0 & 0 & (1-2\nu)/2 & 0 & 0 \\ 0 & 0 & 0 & 0 & (1-2\nu)/2 & 0 \\ 0 & 0 & 0 & 0 & 0 & (1-2\nu)/2\end{bmatrix}}_{\mathbf{C}}\begin{bmatrix}\epsilon_x \\ \epsilon_y \\ \epsilon_z \\ \gamma_{xy} \\ \gamma_{yz} \\ \gamma_{zy}\end{bmatrix} \tag{3.1.15}$$

where C is the stiffness matrix. Hooke's law is then written as

$$\boldsymbol{\sigma} = \mathbf{C}\boldsymbol{\epsilon} \tag{3.1.16}$$

3.1.6 The stress tensor

The stress tensor is defined as

$$S = \begin{bmatrix}\sigma_x & \tau_{xy} & \tau_{xz} \\ \tau_{yx} & \sigma_y & \tau_{yz} \\ \tau_{zx} & \tau_{zy} & \sigma_z\end{bmatrix} \tag{3.1.17}$$

where σ denotes normal stresses and τ denotes shear stresses on an infinitesimal element in a three-dimensional continuum [9]. Figure 3.6 shows the components of the stress tensor and how they are oriented. The first index on each stress component denotes the facet in which the stress component acts and the second index denotes in what direction it acts. Each row of the stress tensor denotes stress components in one plane where the three stresses are orthogonal to each other.

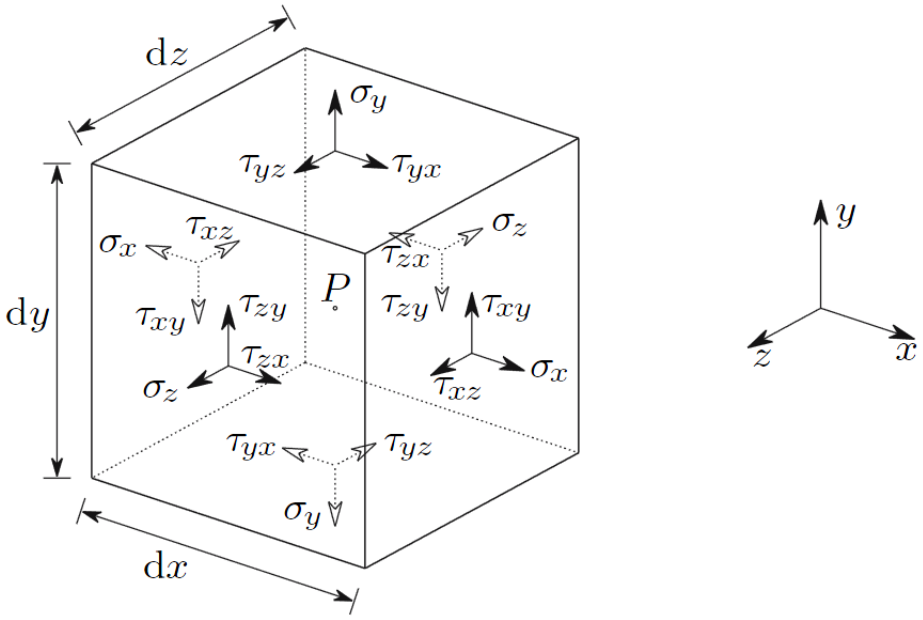

Figure 3.6: *Normal and shearing stresses [8].*

From the condition of equilibrium of rotation it can be shown that

$$\begin{aligned} \tau_{xy} &= \tau_{yx} \\ \tau_{yz} &= \tau_{zy} \\ \tau_{xz} &= \tau_{zx} \end{aligned} \tag{3.1.18}$$

and the stress tensor, S, is thus symmetric [8]

$$S = S^T = \begin{bmatrix} \sigma_x & \tau_{xy} & \tau_{zx} \\ \tau_{xy} & \sigma_y & \tau_{yz} \\ \tau_{zx} & \tau_{yz} & \sigma_z \end{bmatrix} \tag{3.1.19}$$

3.1.7 Principal stresses

Since S is a symmetrical matrix it can be diagonalized, its eigenvalues are all real and if they are all different it has orthogonal eigenvectors. This means that there are always three perpendicular facets where the stress is normal to each facet [8]. The shearing stresses become zero and the only stresses on the element are the normal stresses. These facets are known as principal facets, and their stresses are the principal stresses σ_1, σ_2 and σ_3 in the principal directions: n_1, n_2 and n_3. The principal stresses are illustrated in figure 3.7, and are usually classified by their size where

$$\sigma_3 \leq \sigma_2 \leq \sigma_1 \tag{3.1.20}$$

The sign of the normal stress denotes whether the stress is pointed in or outwards from the infinitesimal element. When analysing stresses in a deformed body the maximal principal stress, σ_1, is used to find the areas of tensile stress and the minimal principal stress, σ_3, is used to find areas of compressive stress.

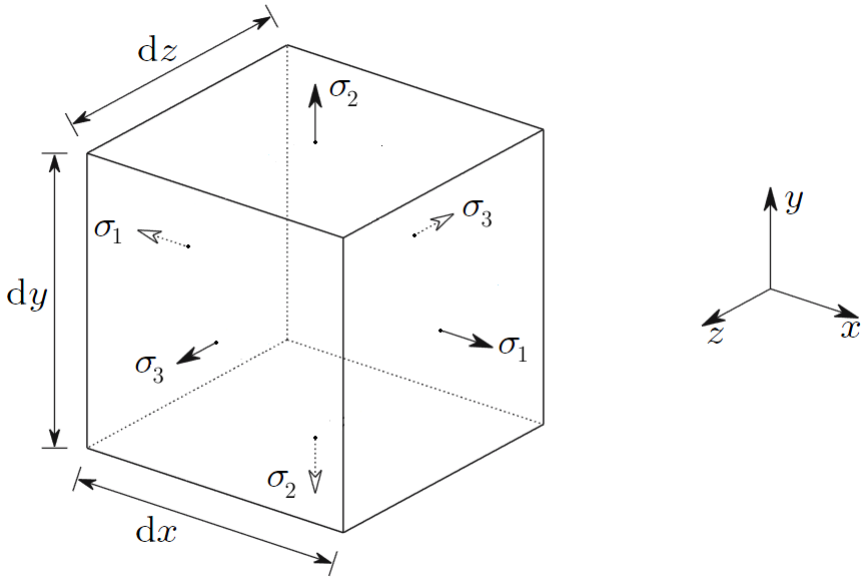

Figure 3.7: *Principal stresses [8].*

3.2 Finite element method

The finite element method, FEM, is a numerical method to find approximate solutions to partial differential equations and integral equations. Instead of solving a continuous problem, the space where an equation is to be solved is divided into a finite set of elements interconnected at nodes, illustrated in figure 3.8. The equation is solved at the nodes and the nodal values are used to interpolate the approximate solution for the continuum [10].

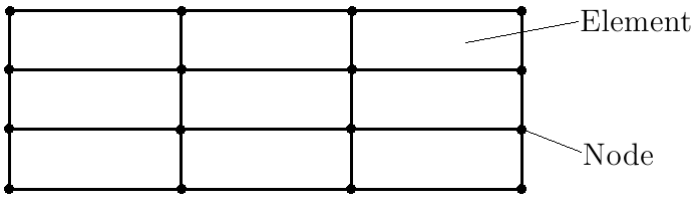

Figure 3.8: *Simple illustration of nodes and elements.*

3.2.1 Stress concentration

Using any model for calculations will give calculation errors, no matter how rigorous the model is. A problem when using FEM is the occurrence of stress concentration, large false stresses appearing at discontinuities of the model. The occurrence of stress concentration can be visualised by comparing the analytical stress results with FEM solutions for a simple beam subjected to an applied load. The beam studied is a homogeneous cantilever beam

with dimensions 50×5×5 m with Young's modulus 50 GPa and Poisson's ratio 0.2 subjected to two different load cases shown in figure 3.16. In the first load case a vertical uniform pressure load is applied to the beam and in the other case a point load is applied at the end of the beam. To show the relation between stress concentration and distance between nodes three different node distances were used, 1.25, 0.625 and 0.3125 m.

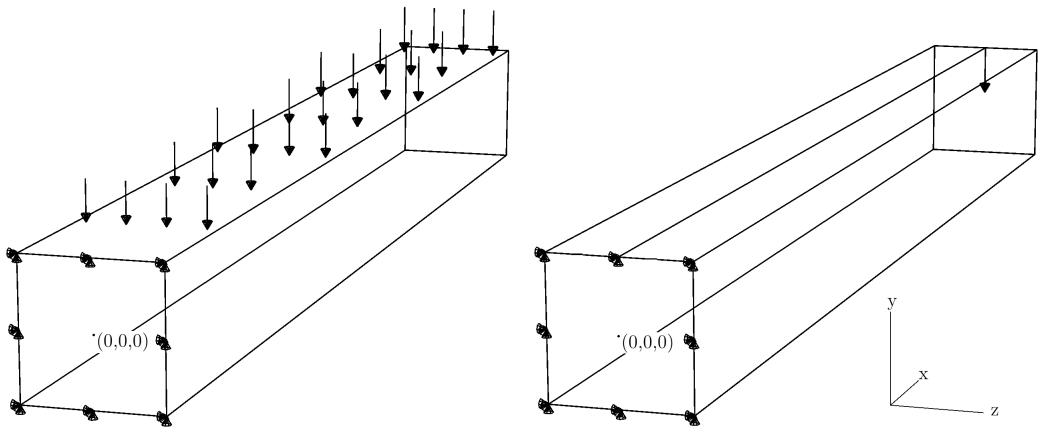

(a) *The pressure load.* (b) *The point load.*

Figure 3.9: *The loads applied to the beam.*

In the pressure load case the normal stress at the surface connected to the foundation is initially studied. The analytical solution of the normal stress, σ_{11}, at this surface can be calculated as [11]

$$\sigma_{11} = \frac{Pb(L-x)^2 y}{2I} \tag{3.2.1}$$

where P is the pressure load, b the width of the beam, L the length of the beam, I the moment of inertia, x the x-coordinate and y the y-coordinate of the point where the stress is calculated. Here the stress was calculated along the vertical center line shown in figure 3.10.

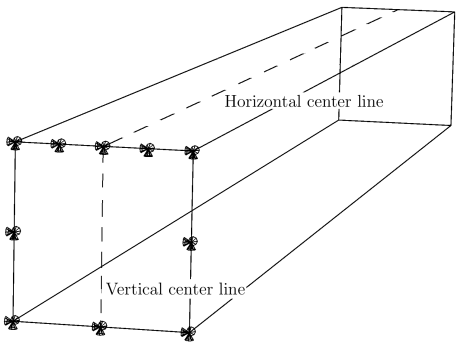

Figure 3.10: *The vertical and horizontal center line of the cantilever beam.*

In figure 3.11a the analytical result is compared to the results from the FEM calculations for the three beams with different element sizes. The relative error, ϵ, is defined as

$$\epsilon = \frac{\sigma_{\text{FEM}} - \sigma_{analytical}}{\sigma_{analytical}} \tag{3.2.2}$$

Table 3.1: *Average relative error of the normal stress.*

Element size (m)	Vertical center line $x = 0$ (%)	Vertical center line $x = 12.5$ (%)	Horizontal center line (%)	Horizontal center line, stress concentration neglected (%)
1.25	11.69	13.35	23.23	20.07
0.625	6.74	4.02	37.72	11.07
0.3125	7.78	1.14	128.0	5.82

where σ_{FEM} is the stress computed with finite element method and $\sigma_{analytical}$ is the analytically computed stress. The relative error of the normal stresses can be seen in figure 3.11b. As illustrated the relative error close to the center of the beam increases as the element size decreases. Further, the average relative error of the beam with smallest element size is somewhat larger than the average relative error for the next smallest element size, as can be seen in table 3.1. This implies that a rougher mesh gives a more accurate result which is contradictive to the knowledge that a more detailed model gives more accurate results.

The same stress was computed at another position in the beam, where $x = 12.5\,\text{m}$. The analytical solution was calculated according to equation (3.2.1) and is compared to the finite element solutions in figure 3.12a. For the relative error in this position, as can be seen in figure 3.12b and table 3.1, ϵ decreases with decreasing element size. A comparison of the relative errors of the stress where $x = 0$ and $12.5\,\text{m}$ indicates that computational errors occur in the boundary of the model, this is known as stress concentration. A larger element size would mitigate this problem but leads to poor estimates of stress in the remainder of the model.

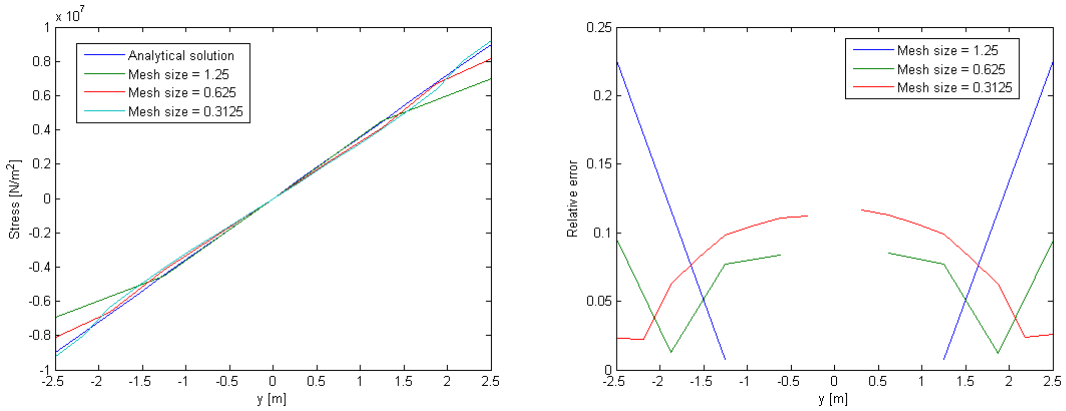

(a) *Normal stress.* (b) *Relative error of the normal stress.*

Figure 3.11: *Normal stress and relative error at the vertical center line, at x =0, when a uniform pressure load is applied to the upper surface of the beam.*

To analyse the stresses introduced by a point load at the end of the beam the normal stress at the horizontal center line on the upper surface of the beam, shown in figure 3.10, was studied. The normal stress is analytically expressed as [11]

$$\sigma_{11} = \frac{Py}{I}(x_{load} - x) \tag{3.2.3}$$

where P is the applied point load in newtons, I the moment of inertia, x_{load} the x-location of the load and x and y are the coordinates of the stress. A comparison of the analytical

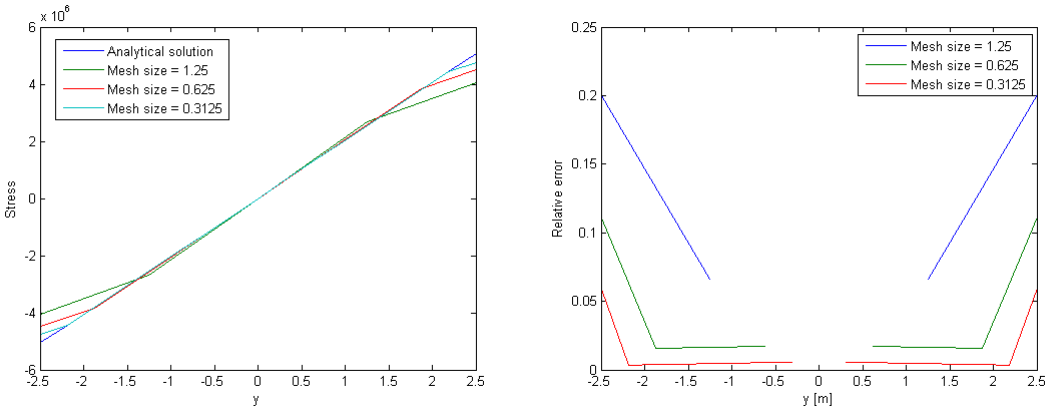

(a) *Normal stress.* (b) *Relative error of the normal stress.*

Figure 3.12: *Normal stress and relative error at the vertical center line, at x =12.5 m when a uniform pressure load is applied to the upper surface of the beam.*

result and the FEM results can be seen in figure 3.13 together with the relative errors. The relative error for all element sizes are relatively stable in the major part of the beam, for the smallest element size $\epsilon < 6\,\%$, for the next smallest element $\epsilon < 11\,\%$ and for the largest element $\epsilon < 21\,\%$ in the region x =[5, 45] m. At the end of the beam where the load is applied the relative error becomes larger, resulting in big average relative errors, as presented in table 3.1. Furthermore, it can be seen that the average relative error increases with decreasing mesh size, as mentioned before a finer mesh should give a more accurate result. The large relative error is due to stress concentration in the area surrounding the point where the load is applied. To get a result closer to the analytical result the points with stress concentration are removed. The stress when neglecting the outermost 5 m, corresponding to 10 % of the beam, is shown in the last column of table 3.1 and now the relative error decreases with decreasing element size.

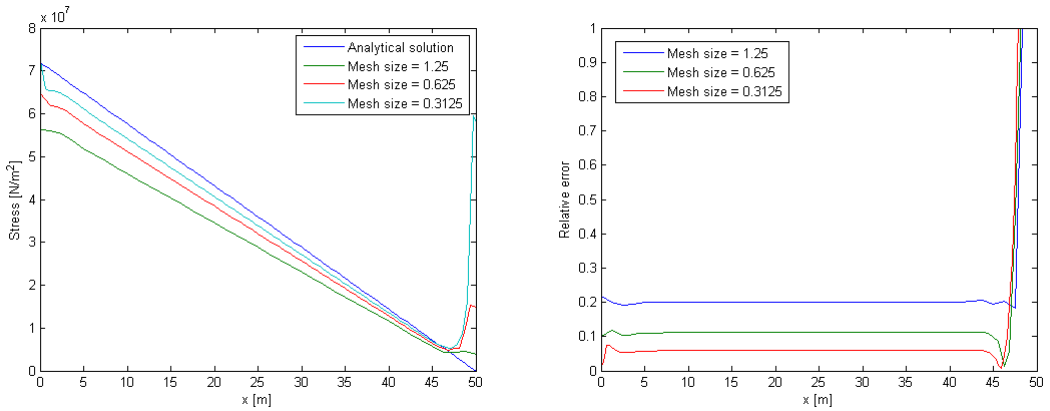

(a) *Normal stress.* (b) *Relative error of the normal stress.*

Figure 3.13: *Normal stress and relative error at the horizontal center line, at y =2.5 m when a point load is applied to the end of the beam.*

From the results of the simple beam problems presented above, it is demonstrated that

stress concentration will occur in discontinuities of the structure or the applied load. Furthermore, the survey showed that by neglecting the region where stress concentration occurs a more accurate result is achieved with FEM-calculations. Stress concentration can not be avoided unless the model is changed or by using larger element sizes. In most cases, changing the model is not an option and the use of larger elements leads to poor estimations in the rest of the model. Consequently, the areas where stress concentration occurs are omitted and a combination of computation and engineering experience must be used to evaluate the results.

3.3 Dams in general

The purpose of a dam is to safely retain and store water. The first dams were built for water storage and irrigation and as civilisations progressed the purpose of dams expanded to include flood control, navigation, sedimentation control, and hydropower. There are numerous types of dams which are generally classified in two groups, embankment dams and concrete dams, based on their construction material [6].

Embankment dams are constructed of earthfill or rockfill. The upstream and downstream face slopes are similar which gives a high construction volume relative to height, see figure 3.14. Embankment dams are generally cheaper since the material used is untreated and locally available from the surroundings, needing little transportation. Embankment dams have proven to be adaptable to a wide range of site surroundings and site circumstances. One of the few disadvantages of embankment dams is their susceptibility for damage by overtopping, creating a need for flood relief using a separate spillway. For technical and economic reasons embankment dams are numerically dominant, accounting for over 85 % of all dams built.

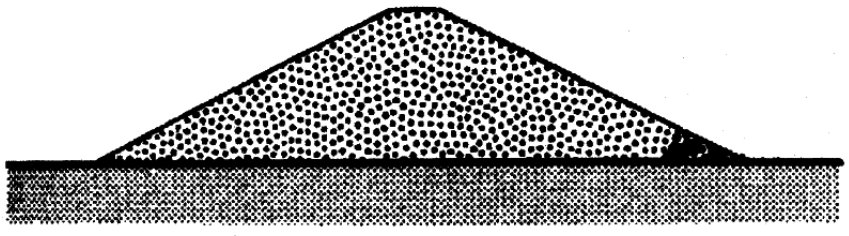

Figure 3.14: *Schematic illustration of an embankment dam [6].*

Concrete dams are generally constructed of mass concrete but older dams made of masonry are also considered to belong in this group. The upstream and downstream face slopes are dissimilar, with a generally steep downstream face and a near vertical upstream face. Since concrete dams have a more slender profile than embankment dams, less material is needed for construction, but economically this is outweighed by the higher cost for concrete. Concrete dams are also more demanding when it comes to foundation conditions, requiring sound rock, and the construction process demands relatively advanced and expensive construction skills. Mass concrete construction is labour-intensive and relatively discontinuous, requiring certain specialised skills. In contrast to embankment dams concrete dams are not sensitive to overtopping during extreme flood conditions. Concrete dams can also accommodate a separate spillway in the crest. A concrete dam can be built to house ancillary

constructions such as outlet pipework or valves.

Concrete dams can be categorised in three main types: gravity dams, buttress dams and arch dams. The gravity dam has a triangular profile with a nearly vertical upstream face and an inclined downstream face, as illustrated in figure 3.15a. The stability of a gravity dam relies entirely on the dam's mass. The gravity dam is the most numerous of the concrete dam types. The buttress dam has a nearly vertical and continuous upstream face and buttresses supporting the structure on the downstream face as can be seen in figure 3.15b. The buttress dam is conceptually considered as a lightened version of the gravity dam and is the least numerous of the dam types presented here.

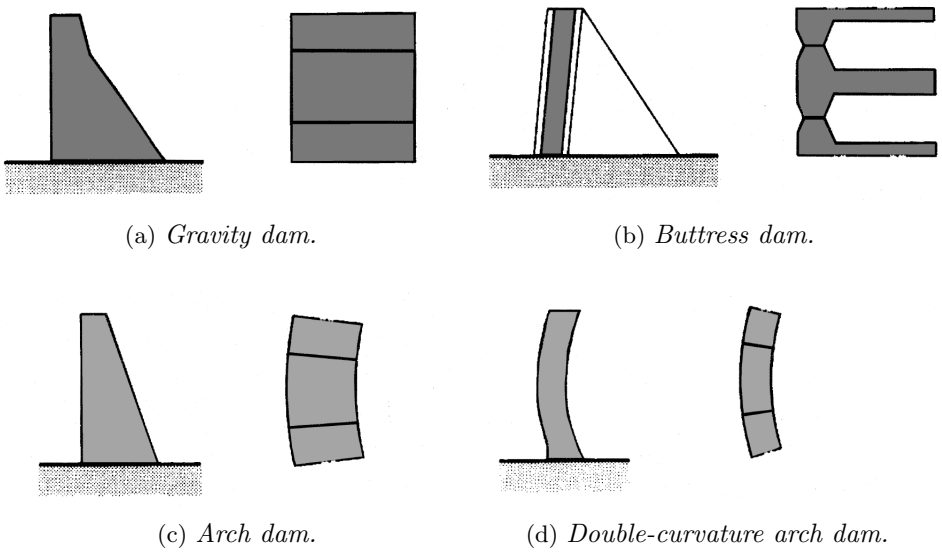

(a) *Gravity dam.* (b) *Buttress dam.*

(c) *Arch dam.* (d) *Double-curvature arch dam.*

Figure 3.15: *Schematic illustrations of four concrete dam types, seen from the side and from above. The upstream face, where the water is contained, is the left side of the dams [6].*

3.3.1 Arch dams

An arch dam has a curved upstream face and functions structurally as a horizontal arch. The water load is thus transmitted to the dam sides where the dam meets the valley, in contrast to the gravity and buttress dams that transmit the load to the ground [6]. This structure is more efficient than other dams, greatly reducing the volume of material needed. A schematic illustration of an arch dam can be seen in figure 3.15c. A version of the arch dam is the cupola or double-curvature arch dam where the dam is curved in the vertical as well as the horisontal plane, see figure 3.15d.

3.4 Loads on concrete dams

Figure 3.16 shows the loads that act on a concrete dam [6]. Although the figure shows a concrete gravity dam, the load diagram is also valid for an arch dam. The loads that act on a dam are divided into three categories, primary, secondary, and exceptional loads, which will be described further in sections 3.4.1-3.4.3.

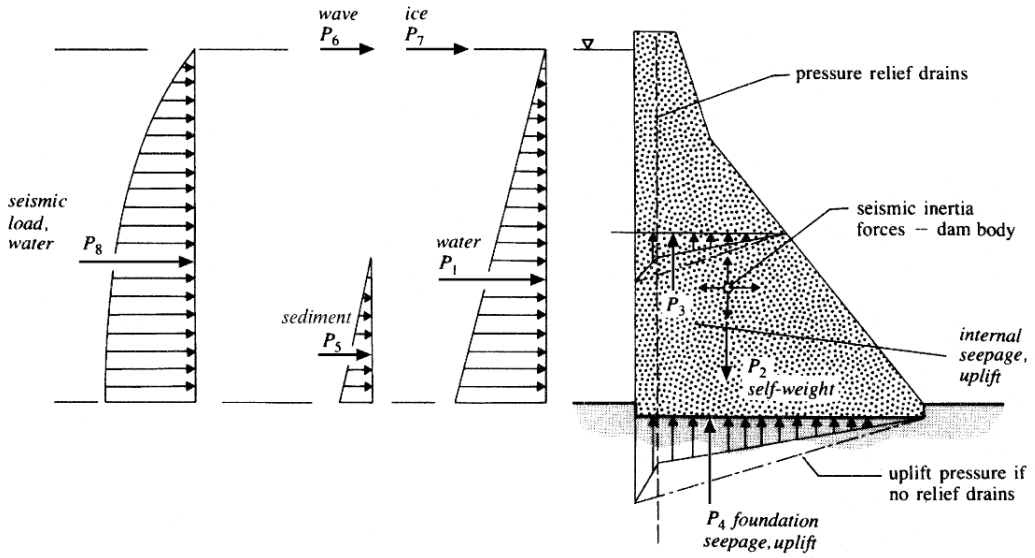

Figure 3.16: *Loads acting on a concrete dam [6].*

3.4.1 Primary loads

Primary loads act on and are of major importance for all dam structures [6]. Loads included are water load, self-weight load, and uplifting load. These loads are always present, although they can vary in magnitude due to external conditions, for example with varying water levels.

Hydrostatic load
The hydrostatic load acting on the dam is the external water pressure, a function of the water depth [6]. The water pressure is expressed as

$$p_{\mathrm{w}} = \rho_{\mathrm{w}} g \Delta h \tag{3.4.1}$$

where ρ_{w} is the water density, g the standard gravity and Δh the water depth.

Self-weight load
The self-weight load is the gravity load acting on the dam [6]. The main material of a concrete dam is concrete, however, there will be some parts such as crest gates and ancillary structures that will have another density and affect the magnitude of the self-weight load.

Uplifting load
The seepage and uplifting load are caused by water penetrating into discontinuities such as joint planes, cracks, and the pore structure of the dam and the foundation. The uplifting load is commonly assumed to be linear and decreases from the external water pressure at the upstream dam face to the external water pressure at the downstream dam face [6]. In arch dams these loads are causing relatively small effects and are therefore generally neglected [12].

3.4.2 Secondary loads

Secondary loads are loads of less magnitude or loads that are of great importance for special dam structures [6]. These loads are time-dependent, some will increase gradually, like

sediment loads, while other will affect the structure only during limited periods of time, like wave and ice loads.

Sediment load
On the upstream face of the dam, accumulating sediment will generate a load acting on the upstream dam face. The sediment pressure is described with Rankin's active earth pressure theory [13]

$$p_s = \gamma_s' \, h_s \tan^2(45^\circ - \Phi/2) \tag{3.4.2}$$

where h_s is the height of the sediment, Φ the friction angle and γ_s' the buoyant unit weight of the sediment, which is the saturated unit weight minus the unit weight of water. The height of the sediment is time-dependent, affected by factors such as sediment concentration and reservoir characteristics [6].

Wave load
This load, caused by waves acting on the dam face, is generally neglected [6]. The reason is that the magnitude is relatively small, the load is irregular and depends on the location. To account for wave load the external water pressure can be adjusted. In cases where the wave force is of importance it can be expressed as

$$P_{wave} = 2\rho_{\mathrm{w}} g H_s^2 \tag{3.4.3}$$

where H_s is the significant wave height.

Ice load
Ice load is only important in locations where thick ice sheets exist for long periods of time [6]. The ice pressure is a function of ice thickness, temperature variation and the restrain at the boundary of the ice sheet. At locations where the ice sheets are expected to be thinner than 0.4 m the ice load is neglected.

Temperature load
Temperature load is caused by the change in volume of the structure when its internal temperature changes [12]. The magnitude of the load is derived from the difference between the measured and closure temperature. The closure temperature is the temperature in the dam structure after cooling. In natural cooling the closure temperature will vary in the dam depending on height, thickness, climatic conditions and more. These variations will introduce stresses in the structure. However, by controlling the cooling the closure temperature could be designed to be uniform or to result in a certain stress distribution.

3.4.3 Exceptional load

The exceptional loads are loads that are hard to predict or have a low probability to occur.

Seismic load
In case of seismic disturbance, loads will be generated due to inertia of the dam and the retained water [6]. A seismic activity will cause both horizontal and vertical accelerations, which both have to be considered.

3.5 Dynamic theory

3.5.1 Earthquakes and seismicity

Dynamic loads on structures can originate from various sources but the most disastrous potential lies in the occurrence of an earthquake. The degree of importance of earthquake load is related to the probable intensity and likelihood of occurrence, also known as the seismicity [14]. The seismicity of a region determines to what extent the earthquake load will determine the design of structures in that region. The principal directory of seismicity is the recorded history of earthquakes in the region of interest. In China, records have been kept that are believed to include major destructive seismic events for 3 000 years, thus there is considerable knowledge about the seismicity of China. In large parts of the world earthquake recordings remained incomplete and inconsistent until the 1960's when measurements became standardised and more widespread, making it possible to study seismicity on a global scale. From the compilation of these data it is evident that earthquake occurrences are not uniformly distributed over the surface of the earth, instead earthquakes are concentrated along lines defining the boundaries between the tectonic plates of the earth's crust.

3.5.2 Earthquake faults and waves

The rock near the surface of the earth is not as rigid and motionless as it seems to be. Rock masses move relative to each other creating strains when the rock bends like elastic-plastic material [14]. When the deformations and stresses in the rock reaches the breaking strength of the material a rupture in the crest occurs and the rock masses slide relative to each other. It is this rupture, known as geological failure, that causes an earthquake. The failure releases strain energy which is transmitted through the earth in vibratory elastic waves radiating outwards from the point of rupture.

The waves emerging from the rupture is what constitutes the earthquake and two wave types can be identified. "P" waves, or Primary waves, travels most rapid through the rock, arriving first at any given point. In "P" waves the material particles are transferred in the same path as the wave propagation, creating alternating tension and compression deformation. In "S" waves, or Secondary waves, the material particles move perpendicular to the wave propagation path inducing shear deformation. When the wave energy propagates near the surface two other wave types can be identified. Rayleigh waves are similar to the "P" waves in that they are tension-compression waves except for that their amplitude declines with distance from the surface. Love waves are the equivalent of the "S" waves when energy is transferred close to the surface, they are shear waves diminishing rapidly with distance below the surface. The different wave types are illustrated in figure 3.17.

3.5.3 Measures of earthquake size

The size of an earthquake can be quantified in two ways, by its magnitude and by its intensity [14]. The magnitude, often expressed in the Richter scale, depicts the amount of strain energy released at the source. In the Richter scale, the the magnitude, M, and the released energy, E, have been empirically related by the formula

$$\log E = 11.8 + 1.5\,M \tag{3.5.1}$$

This relation states that the energy increases by a factor of 32 with each unit of magnitude increased. It has also been empirically observed that earthquakes of magnitude greater than 5 on the Richter scale have potential to produce ground motion harmful to structures.

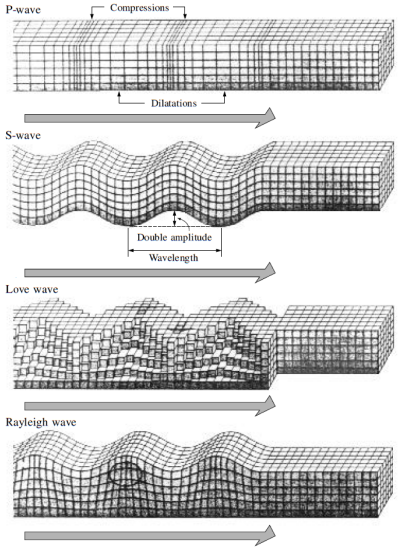

Figure 3.17: *Illustrations of the ground motion in different wave types. The arrows denote the direction of the waves [14].*

Of more importance when designing structures in seismic areas is the expected earthquake intensity. The magnitude of the earthquake is only a measure of the earthquake at its source, while the distance from the source is an equally important factor on how structures are affected. The earthquake intensity is the severity of ground motions or damage caused by an earthquake at any given point. Two of the scales used are the Mercalli scale or the Modified Mercalli scale which are 12-point scales ranging from I, not felt by anyone, to XII which means total destruction.

Earthquake forces for most structures are characterised by the time history of the ground acceleration [15]. Strong-motion acceleration is characterised by amplitude, duration, and frequency content. Although it is difficult to specify the overall strength of motion correctly with a single number, a common measure of acceleration amplitude is the peak acceleration. It is easily and accurately determined from the accelerogram without data processing. It has also proven to be a useful measure, though it can be quite imprecise if narrow spikes of acceleration occurs, spikes that determine the peak acceleration but do not signify the structural response for the majority of structures. The peak ground velocity and peak ground displacement can also be used as a measure for the earthquake at a specific site. They both require data processing since it is the acceleration that is measured, and neither of them is a better indicator for structural response, with a few exceptions, than the peak ground acceleration.

The frequency content of the acceleration characterises the way the acceleration contains energy at different frequencies. Different frequencies are more hazardous to some structures than to others, due to the different natural frequencies of different structures.

3.5.4 Structures under dynamic load

The motion of a structure with a lumped mass m supported by a massless structure of stiffness k in free vibration subjected to a time-dependent external force $p(t)$ is governed by the equation

$$m\ddot{u} + ku = p(t) \tag{3.5.2}$$

where u is the displacement of the lumped mass and $\ddot{u}$ its acceleration [16]. The same equation can also be written in the form

$$f_I + f_S = p(t) \tag{3.5.3}$$

where $f_I = m\ddot{u}$ is the inertia force and $f_S = ku$ the elastic force. When a structure vibrates energy dissipates by various mechanisms, damping the motion. The damping force f_D is proportional to the velocity of the structure,

$$f_D = c\dot{u} \tag{3.5.4}$$

where $\dot{u}$ is the velocity of the structure mass and c is the viscous damping coefficient. The equation governing the movement of a structure when damping is included becomes

$$m\ddot{u} + c\dot{u} + ku = p(t) \tag{3.5.5}$$

$$f_I + f_D + f_S = p(t) \tag{3.5.6}$$

Unlike the stiffness of a structure the damping coefficient can not be calculated from the dimensions and material properties of the structure, since the energy dissipation in structures is caused by several different mechanisms. The approach used is to idealize the multitude of damping forces by equivalent viscous damping.

Equation (3.5.6) describes the motion of a structure with only one degree of freedom, DOF. Most structures have multiple degrees of freedom. Consider a structure being idealised to consist of interconnected nodes with a total of N DOFs, the dynamic equilibrium for each DOF may be expressed as

$$\begin{aligned} f_{I1} + f_{D1} + f_{S1} &= p_1(t) \\ f_{I2} + f_{D2} + f_{S2} &= p_2(t) \\ &\vdots \\ f_{I,N} + f_{D,N} + f_{S,N} &= p_N(t) \end{aligned} \tag{3.5.7}$$

or in matrix form they are expressed as

$$\mathbf{f}_I + \mathbf{f}_D + \mathbf{f}_S = \mathbf{p}(t) \tag{3.5.8}$$

which generalises equation (3.5.5) to

$$\mathbf{m\ddot{u}} + \mathbf{c\dot{u}} + \mathbf{ku} = \mathbf{p}(t) \tag{3.5.9}$$

where $\mathbf{m}$ is the mass matrix, $\mathbf{c}$ the damping matrix, $\mathbf{k}$ the stiffness matrix and $\mathbf{p}(t)$ is the matrix containing the applied forces [14]. The stiffness influence coefficient k_{ij} of the stiffness matrix is the force required at DOF i for a unit displacement at DOF j. The damping influence coefficients c_{ij} in the damping matrix are defined in a similar way, c_{ij} is the external force in DOF i due to unit velocity in DOF j. The mass influence coefficient m_{ij} is the external force in DOF i due to unit acceleration along DOF j. The stiffness matrix $\mathbf{k}$ and the mass matrix $\mathbf{m}$ are both symmetric

$$\begin{aligned} k_{ij} &= k_{ji} \\ m_{ij} &= m_{ji} \end{aligned} \tag{3.5.10}$$

Furthermore, if the mass is idealised as concentrated at the nodes of the discretized structure, the mass matrix becomes diagonal

$$\begin{aligned} m_{ij} &= 0, \qquad j \neq i \\ m_{jj} &= m_j \text{ or } 0 \end{aligned} \tag{3.5.11}$$

where m_j is the mass associated with the jth translational DOF and for a rotational DOF $m_{jj} = 0$. Simplifying a structure with node-concentrated masses is usually a satisfactory assumption.

Rayleigh damping

Since it is impractical to determine the coefficients of the damping matrix from the structure dimension, structural member size and the damping of structural materials used the damping is specified by numerical values for the modal damping ratios [16]. The modal damping ratios contain all energy-dissipating mechanisms and they are sufficient for analysis of linear systems with classical damping.

A simple way to formulate a damping matrix is by making it proportional to either the mass or stiffness matrix since they are both orthogonal to the undamped mode shapes, the damping matrix can thus be given by

$$\mathbf{c} = a_0\,\mathbf{m} \quad \text{or} \quad \mathbf{c} = a_1\,\mathbf{k} \tag{3.5.12}$$

with proportionality constants a_0 and a_1 [14]. For mass proportional damping the damping ratio, ξ, is inversely proportional to the frequency, while for stiffness proportional damping the damping ratio is directly proportional to the frequency;

$$\xi_n = \frac{a_0}{2\omega_n} \quad \text{or} \quad \xi_n = \frac{a_1\omega_n}{2} \tag{3.5.13}$$

Although, neither of these damping matrices are suitable when considering a system with multiple degrees of freedom. A combination of the mass and stiffness matrices gives obvious improvements,

$$\mathbf{c} = a_0\mathbf{m} + a_1\mathbf{k} \tag{3.5.14}$$

this is known as Rayleigh damping. The relation between damping ratio and frequency in Rayleigh damping is

$$\xi_n = \frac{a_0}{2\omega_n} + \frac{a_1\omega_n}{2} \tag{3.5.15}$$

where ω_n is the frequency of the n:th mode. The relation between damping ratio and

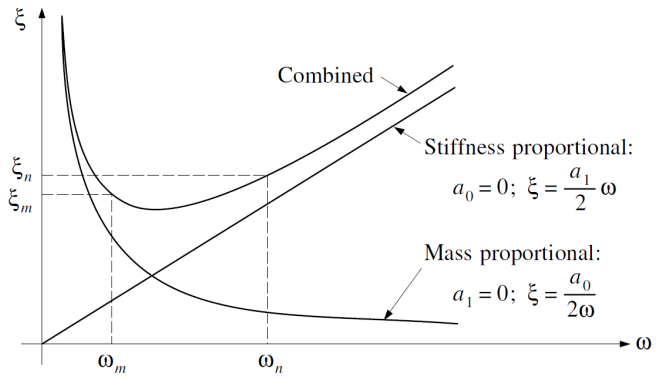

Figure 3.18: *Relation between damping ratio and frequency in Rayleigh damping [14].*

frequency as in equations (3.5.13) and (3.5.15) can be seen in figure 3.18. If the damping ratios ξ_m and ξ_n associated with the two frequencies ω_m and ω_n are known the two Rayleigh damping factors can be evaluated by solving the two equations, in matrix form

$$\begin{Bmatrix} a_0 \\ a_1 \end{Bmatrix} = 2\frac{\omega_m\omega_n}{\omega_n^2 - \omega_m^2} \begin{bmatrix} \omega_n & -\omega_m \\ -1/\omega_n & 1/\omega_m \end{bmatrix} \begin{Bmatrix} \xi_m \\ \xi_n \end{Bmatrix} \tag{3.5.16}$$

Since accurate and detailed information about how damping ratio varies with frequency seldom is available, it is often assumed that the same damping ratio applies for both frequencies

$$\xi_m = \xi_n \equiv \xi \tag{3.5.17}$$

If this is the case, the proportionality constants can be evaluated with a simplified version of equation (3.5.16)

$$\begin{Bmatrix} a_0 \\ a_1 \end{Bmatrix} = \frac{2\xi}{\omega_m + \omega_n} \begin{Bmatrix} \omega_m \omega_n \\ 1 \end{Bmatrix} \tag{3.5.18}$$

The first frequency ω_m is generally taken as the fundamental frequency of the multi degree of freedom system (MDOF), while ω_n is set among the higher frequencies of the modes contributing significantly to the dynamic response. The desired damping, ξ, is obtained for these two modes and for the frequencies between ω_m and ω_n the damping is somewhat lower, as seen in figure 3.18. Modes with frequencies greater than ω_n will have damping ratios that increases above ξ with frequency. Thus the response of high frequency modes is eliminated by the high damping ratio.

Westergaard added mass

During an earthquake the water in the reservoir is set in motion, resulting in hydrodynamic forces exerted on the upstream dam face. As proposed by H.M. Westergaard the hydrodynamic forces can be seen as equivalent to inertia forces of a volume of water attached to and moving back and forth with the dam while the rest of the reservoir water remains inactive [17]. For analysis of a dam idealised as a 2-dimensional rigid monolith with vertical upstream face the body of water attached to the dam is proposed to have a parabolic shape, as shown in figure 3.19. The added mass of water at location i, $m_{added,i}$, is obtained by multiplying the mass density of water, ρ_w by the volume of water tributary to point i in the formula

$$m_{added,i} = \frac{7}{8}\rho_w A_i \sqrt{H(H - z_i)} \tag{3.5.19}$$

where H is the water depth, z_i the height above the dam base and A_i the tributary surface area at point i. The Westergaard added mass is then added together with the mass of the dam at each point of the dam surface

$$m_{total,i} = m_{dam,i} + m_{added,i} \tag{3.5.20}$$

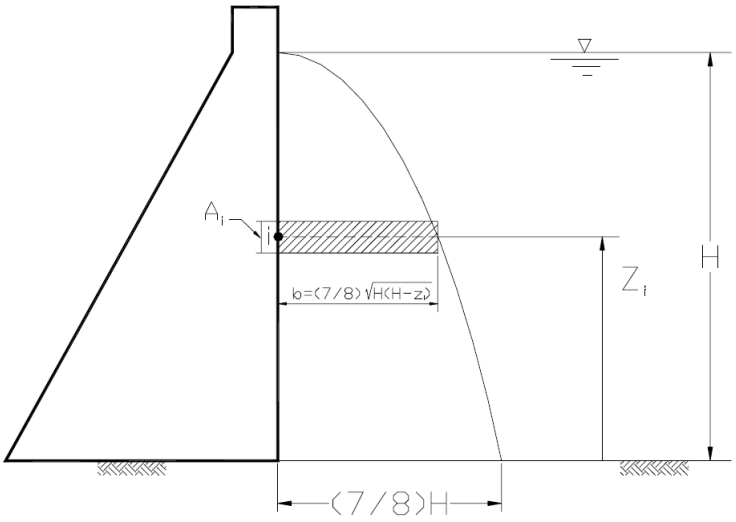

Figure 3.19: *Added mass for a dam idealised as a 2D rigid monolith with vertical upstream face [17].*

Design criteria for earthquake loads

Since earthquake probabilites are relatively small, damages to the structure are accepted, hence the magnitude of stresses allowed during an earthquake are generally larger than otherwise [18], [19]. The magnitude of the allowed damages is determined by the probability of the earthquake. For example, according to the US Army Corps of Engineers [18], for ground motions that have a 50 % probability of exceedence during the service life, which is generally around 100 years, the structure is expected to be operable immediately after. As a comparison, for ground motions that has a 10 % chance of being exceeded in 100 years, damage to the structure may be significant, but concentrated to limited regions and the damage must be repairable to stop further damage by static loads. Although tensile stresses as well as compressive stresses are evaluated for earthquake loads, the most important measure is the tensile stress. This since the safety and serviceability of large plain concrete structures is controlled by the tensile behaviour and cracking of the concrete.

Chapter 4:

Method

The dam was modeled in the software Patran 2007 and produced at the Department of Hydraulic Engineering at Tsinghua University, Beijing. The model consisted of two parts, the dam and the foundation. The dam and the general characteristics of the valley were modeled after their actual dimensions and the foundation can be seen as a block with height 600 m, length 760 m and width 1077 m where the valley is carved out. The foundation is thus twice as wide and twice as high as the dam.

The element type used had eight nodes. The number of nodes in the model was 40 261 and the number of elements became 35 742. In the y-direction of the dam there were always six elements and a typical distance between nodes in the x- and z-direction was 10–20 m. The distance between nodes in the foundation was smaller closest to the dam and grew larger further away from the dam where less computation accuracy was needed. The meshing, where the nodes and elements are appointed, was also done in Patran 2007 and the meshed model can be seen in figure 4.1.

The material of the dam was assumed to be homogenous consisting only of concrete, thus inhomogeneities such as reinforcement bars and cavities within the dam were disregarded. The foundation was also regarded as homogenous, only consisting of rock. The material properties used for concrete and rock can be seen in table 4.1. Both concrete and rock were assumed to behave as linear elastic materials.

To keep the model of the dam and the foundation in place during simulations boundary conditions on the foundation had to be used. The bottom surface of the foundation was fixed in z-direction, making it possible for the nodes to move within the xy-plane but not away from it. The other sides of the foundation, except for the valley and top surfaces, were also fixed to stay within the xz-plane or the yz-plane, see figure 4.2.

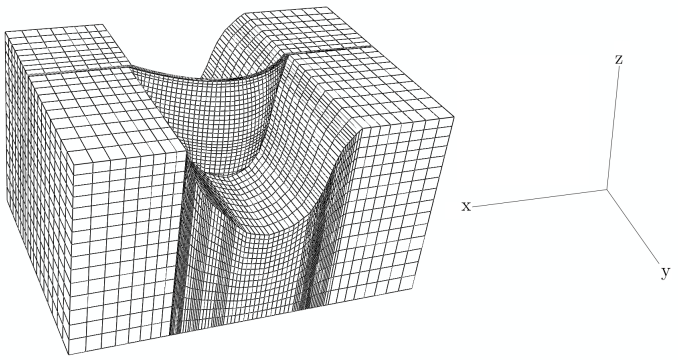

Figure 4.1: *Model of the Jinping I dam.*

Table 4.1: *Material specifications for concrete and rock.*

Property	Concrete	Rock
Density (kg/m^3)	2 400	-
Elastic modulus (GPa)	24	26
Poisson's ratio (-)	0.16667	0.27
Linear expansion coefficient ($^\circ$C^{-1})	$0.1{\cdot}10^{-4}$	-
Compressive strength (MPa)	9	-
Tensile strength (MPa)	1.2	-

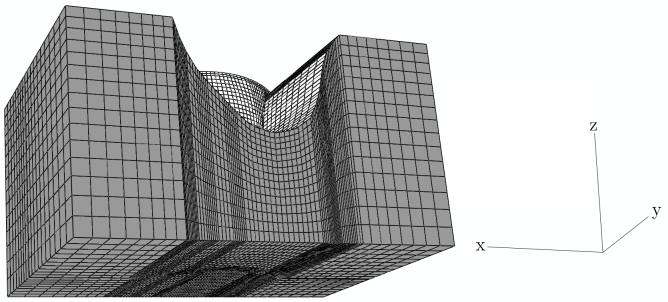

Figure 4.2: *Boundary conditions of the foundation, grey surfaces depicting nodes that only can move within their plane.*

All simulations in both static and dynamic conditions were done in the software Abaqus/CAE 6.9. Specific data on the Jinping I dam dimensions, material properties, water levels, load parameters, temperature distributions and also the earthquake acceleration data were all provided by the Department of Hydraulic Engineering at Tsinghua University.

4.1 Static conditions

The first part of the analysis considers the dam under static conditions, where the loads are seen as time-independent and can thus be applied all at once. Five different loads are considered in the static case: upstream and downstream hydrostatic pressure, self-weight load, sediment load, and temperature load, illustrated in figure 4.3. The hydrostatic load was applied according to equation (3.4.1) on page 21. Four different water conditions were considered; normal, dead, design flood and check flood water level. The upstream and downstream water levels are specified for each water level case in table 4.2, together with their expected return periods, where applicable. The normal water level is expected to be dominant over time, while the other water levels are rarely occuring. For all water levels below the dead water level the hydropower plant will be shut down and no power will be produced. The occurrence of dead water level is not defined, it is generally different for different hydropower plants and if the reservoir is big enough there will be no occurrence [19].

The self-weight load is only applied to the dam, the gravity load of the foundation has been constant for a long time and applying gravity to the foundation would give false deformations. This massless rock foundation model can adequately represent the effects of rock supporting the structure [18]. The sediment load was applied to the upstream face of the dam according to equation (3.4.2), page 22, with the buoyant unit weight of the sediment $\gamma_s' = 5\,\mathrm{kN/m^3}$, height $h_s = 1644.1\,\mathrm{m}$ and friction angle $\Phi = 0\,^\circ$. When considering the tem-

Table 4.2: *Characteristic water levels.*

Conditions	Upstream water level, asl (m)	Downstream water level, asl (m)	Return period (years)
Normal water level	1880	1641.7	-
Dead water level	1800	1641.7	Undefined
Design flood water level	1880.26	1641.7	2000
Check flood water level	1883.46	1658.8	5000

perature load, only the highest and lowest temperature differences in a year with respect to the closure temperature were considered. The temperature in the dam was set to vary with height and also between upstream and downstream faces, it was thus assumed that the temperature was constant on a horizontal line on the dam face. Mean temperatures as a function of height, T_m, and the temperature differences between upstream and downstream faces, T_d are attached in table A.1 in Appendix A. With the given values for temperature, the temperature in each node was linearly interpolated for all nodes in the dam.

The uplift load was disregarded since this load is generally very small for arch dams, the wave- and iceload are generally very small compared to the other loads for high dams and were also neglected.

When simulating the static conditions six different load cases were considered combining the four water levels and the two temperature loads. The load cases studied here are the ones generally studied for arch dams and are presented in table 4.3.

Table 4.3: *Load cases with their respective case names used in the report.*

Water level	Maximum temperature	Minimum temperature
Normal water level	CASE 1	CASE 2
Dead water level	CASE 3	CASE 4
Design flood water level	CASE 5	
Check flood water level	CASE 6	

4.2 Dynamic conditions

Under dynamic conditions the structure is subjected to time-dependent loads in addition to the static loads. In this analysis the dynamic load applied to the dam was the load from an earthquake. The static load case used is CASE 1 and the static and dynamic loads are applied simultaneously. The probability for the occurrence of flood or dead water level is very low, just as the probability for an earthquake, making the probability of them occurring at the same time even lower.

The added mass matrix was calculated according to equation (3.5.19) on page 27. With numbers specific for the Jinping I dam the expression becomes

$$m_{added} = \begin{cases} 875\sqrt{H_0(H_{max} - z)} & \text{if } 1580 \leq z \leq H_{max} \\ 0 & \text{if } H_{max} < z \leq 1885 \end{cases} \tag{4.2.1}$$

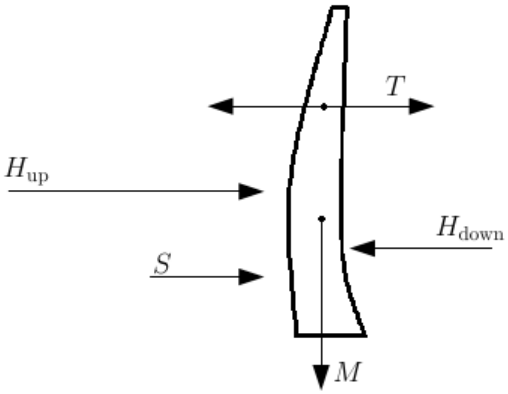

Figure 4.3: *Loads applied to the dam under static conditions. H_{up} and H_{down} are the upstream and downstream hydrostatic loads, S the sediment load, M the self-weight load and T the temperature load.*

where H_0 is the water height of 300 m and H_{max} is the normal water level of 1880 m. The calculations were performed in Patran 2007.

A modal analysis of the dam structure was performed in Abaqus to find the modal frequencies. The frequencies ω_1=7.12 rad/s and ω_5=15.1 rad/s were chosen for calculation of the Rayleigh damping, according to equation (3.5.15) on page 26. Using a damping ratio of $\xi = 5\,\%$, a reasonable estimate of the dynamic response of concrete hydraulic structures near yield and cracking [18], in equation (3.5.18), page 27, resulted in damping factors a_0=0.484 and a_1=0.0045.

The time-dependent load is defined by the ground acceleration in x, y and z-directions. The dynamic load was applied to the boundaries of the foundation for 20 s and the accelerations are visualised for reference in figure 4.4. The peak ground acceleration used is 1.97 m/s^2, the normalised acceleration of the earthquake in the cross and stream direction were multiplied by 1.97 and the normalised acceleration in the vertical direction by $\frac{2}{3}$ of the peak ground acceleration [20], that is 1.31. The elastic modulus is strain rate sensitive and the relation between the static and dynamic modulus used is, [21]

$$E_{dynamic} = 1.3 \cdot E_{static} \tag{4.2.2}$$

4.3 Stress and displacement control

The most extreme values of stress in the dam are found on its surfaces. In the static analysis the maximal and minimal principal stresses are evaluated at the upstream and downstream faces of the dam. The stress data from Abaqus was interpolated and then plotted in MatLab. Due to stress concentration, computational errors giving large and incorrect stresses, in the interface between the dam and the foundation, the nodes connecting the dam and the foundation are omitted from the stress analysis. The maximum and minimum stress values were evaluated in two ways. The first extreme values were evaluated from the remaining nodes and the second extreme values were evaluated from the interpolated data when stress concentration areas had been removed in a second step. This area, a region along the dam-foundation interface with a thickness of 5 % of the dams height, was removed

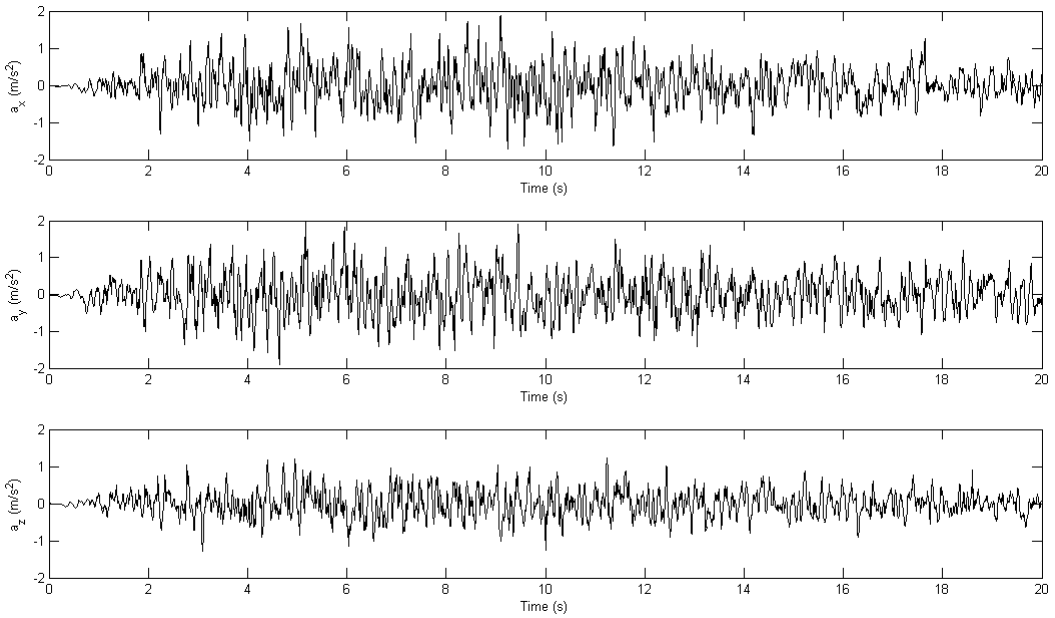

Figure 4.4: *Ground acceleration of the design earthquake.*

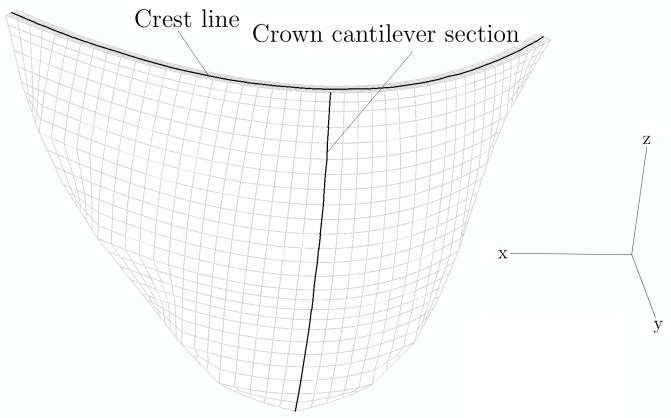

Figure 4.5: *Crest line and crown cantilever section.*

before evaluating the second extreme values.

The displacement of the dam is monitored in the y-direction, that is roughly normal to the dam face, along two different lines. The first line is situated at the middle of the crest and the second at the center line of the upstream dam face called the crown cantilever section, see figure 4.5.

In the dynamic analysis the stress was evaluated at the upstream and downstream surfaces. The maximum value of the maximal principal stress and the minimum value of the minimal principal stress over the whole time span was extracted in each node. The displacement was evaluated at the crest line and crown cantilever section, where the extreme values, downstream as well as upstream, over the whole time-span are shown. The minimum displacement of each node on the upstream surface was also evaluated. Time-dependent displacement was evaluated at two locations on the crown cantilever section, the uppermost node and the mid-node. In addition to the deformation the whole dam structure will move during the simulated earthquake. To get the displacement from the deformation of the dam

the bottom node on the upstream face is used as a reference point. The maximum values over the whole time span in both negative and positive directions, that is, the downstream and upstream directions respectively, were extracted. Otherwise, the data processing was performed as in the static case.

4.4 Analysis method

To analyse the stability of the Jinping I dam the stresses were compared to both the strength of concrete and to results from a similar arch dam. The methods are presented below.

4.4.1 Strength of concrete

In the comparison to the strength of concrete it was investigated if the maximal principal stress exceeded the tensile strength of concrete and if the minimal principal stress exceeded the compressive strength of concrete. As mentioned in section 3.5.4, the tensile behaviour controls the safety of large plain concrete structures, thus greater importance was given to measures of tensile stress in the analysis.

4.4.2 Comparison of another arch dam

To evaluate the results of the Jinping I dam the stresses and deformations were compared to similar FEM-analyses of another arch dam in China, the Ertan dam. The Ertan dam is an arch dam located at the Yalong River in the Sichuan province and has been in operation since 1999 [21]. It is 240 m high and 775 m wide at the crest, with a base thickness of 56 m and a crest thickness of 11 m. Material parameters of the Ertan dam can be found in table 4.4. The dynamic load applied to the Ertan dam was an earthquake with a peak ground acceleration of 2.58 m/s^2. The probability of an earthquake of this size to occur at the Ertan dam is 2 % in 100 years. Since this probability is equal to the probability of the earthquake used for the Jinping I dam to occur, the damages and stresses of the two dams, although subjected to different loads, are comparable. Stress and displacement results of the Ertan dam under different loading conditions are found in Appendix B.

Table 4.4: *Material specifications for concrete in Ertan dam.*

Property	Concrete
Density (kg/m^3)	2 400
Elastic modulus (GPa)	21
Poisson's ratio (-)	0.17
Linear expansion coefficient ($°C^{-1}$)	$0.1 \cdot 10^{-4}$

Chapter 5:

Results

5.1 Static conditions

The static analysis included six different load cases, shown in table 4.3. For each load case the maximal and minimal principal stress at the upstream and downstream faces have been evaluated and are presented in contour plots, shown from a downstream view. Furthermore, the displacement of the crown cantilever section and the crest line have been evaluated. To verify the results from the Jinping I dam they were compared to similar simulated results of the Ertan dam [21]. When these were available, the contour plots of the stress calculations of the Ertan dam can be found in Appendix B.

5.1.1 CASE 1 - Normal water level, maximum temperature

Figure 5.1 shows contour plots of the maximal and minimal principal stress at the upstream face, for CASE 1. Indicated in the figure are also the extreme values of the maximal and minimal principal stresses, since the extreme values are the critical stresses that the dam has to resist to prevent a failure. The maximum maximal principal stress, indicated with a red star in figure 5.1a, corresponds to the largest tension at the upstream dam face. Another maximum value was found when areas of stress concentration were removed, estimated as 5 % of the dam height. The secondary maximum was found to be situated at the upper part of the dam close to the stress concentration region, indicated with a blue star in figure 5.1a.

The red star in figure 5.1b indicates the minimum minimal principal stress, which is the location of the largest compression on the upstream surface. Since the extreme value of the minimal principal stress is not found on the boundary between the dam and the foundation there were no need to search for a second extreme value. The extreme value found was not due to stress concentration and if stress concentration has occurred, it has not contributed with any stress of greater magnitude than the value found. All extreme values are summarised in table 5.1.

The upstream faces of the Jinping I dam and the Ertan dam, illustrated in figure B.1 in Appendix B, have similar contour plots with extreme values located in the same regions. In table 5.2 the extreme values of the Ertan dam are presented. The extreme value of the minimal principal stress correspond well for the two dams. On the other hand, the maximal principal stresses differ, where the Ertan dam has an apparently larger maximum, which is believed to be due to stress concentration at the edge of the dam. Of more importance are the second maximum values for the dams which show a slightly lower value for the Jinping I dam.

The minimum value of the minimal principal stress had smaller magnitude than the com-

pressive strength of concrete, presented in table 4.1. On the other hand, the maximum value of the maximal principal stress exceeded the tensile strength of concrete. However, when the stress concentration region was removed the second maximum value was in the safety region of the strength of concrete.

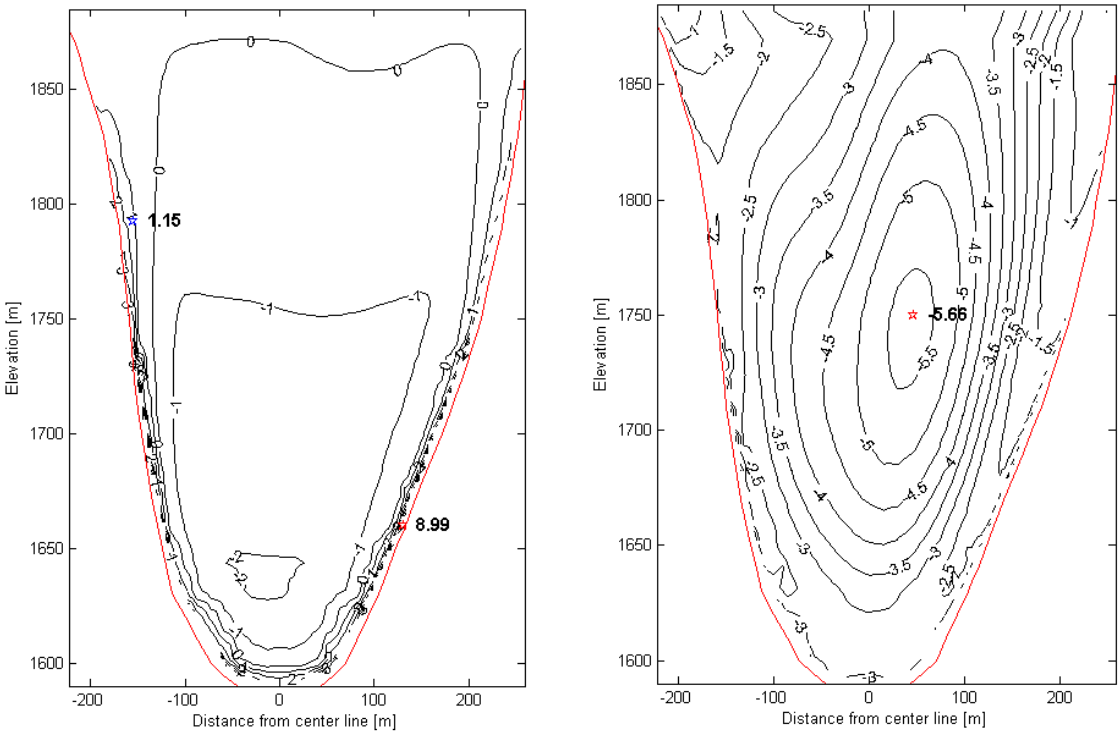

(a) *Maximal principal stress [Mpa].* (b) *Minimal principal stress [Mpa].*

Figure 5.1: *Principal stress at the upstream dam face in CASE 1. The stars denote extreme values.*

The calculated stresses at the downstream face is shown in figure 5.2. The maximum tension was found at the bottom of the dam and the alternative maximum was also located in this area, indicated by a blue star in the figure. The compression was largest near the edge of the right side of the dam. From the edge the stress increases monotonically towards the inner of the dam and a secondary minimum was found close to the minimum value just outside the stress concentration region. The second minimum together with a small area around it exceeds the compressive strength of concrete.

A comparison of the minimal principal stress at the downstream face of the Jinping I dam and the Ertan dam, illustrated in figure B.2b, indicate that the distribution have the same pattern and that the minimum values are comparable. The Jinping result of the maximal principal stress is not as easy to compare with the Ertan dam, shown in figure B.2a. However, it can be concluded that the maximal principal stress is consistently low in both dams. Both the extreme and the second extreme value for the Jinping I dam are slightly larger than for the Ertan dam and have different locations. Although the maximum values are larger than for the Ertan dam they are lower than the allowed values for the strength of concrete.

The displacement of the crest line and the crown cantilever section are shown in figure 5.3.

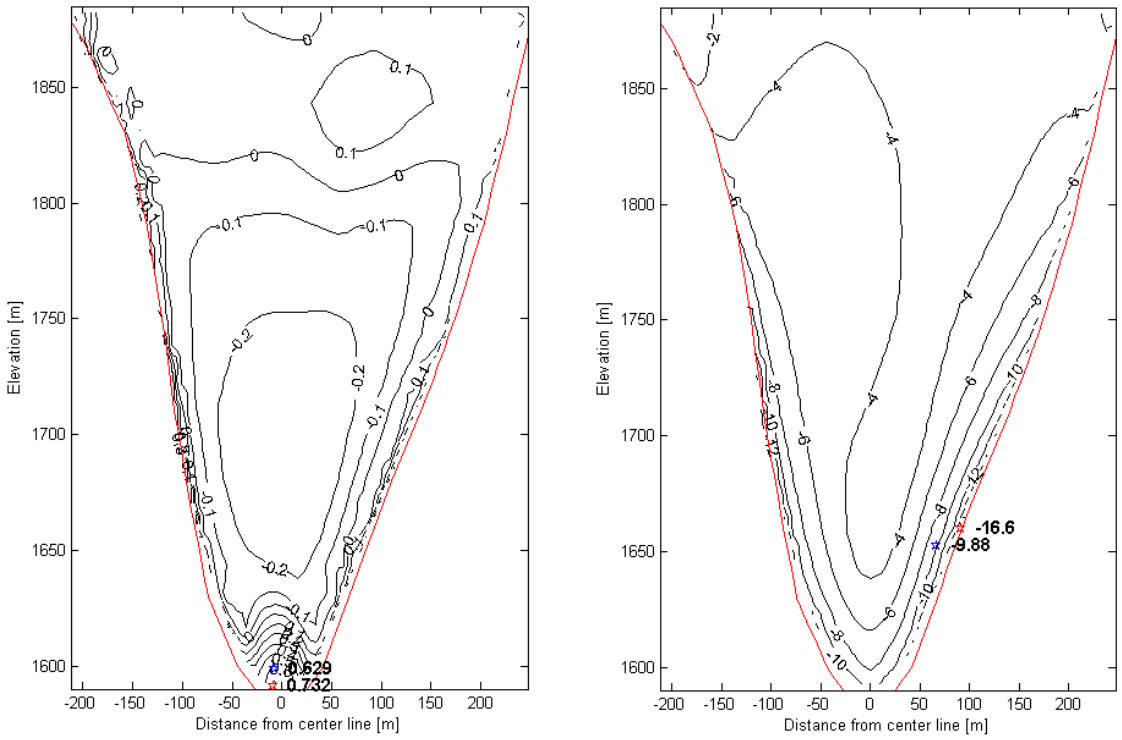

(a) *Maximal principal stress [Mpa].* (b) *Minimal principal stress [Mpa].*

Figure 5.2: *Principal stress at the downstream dam face in CASE 1. The stars denote extreme values.*

A negative value indicates that the displacement is downstream and the largest value is presented in table 5.3.

The displacement of the crown cantilever section is evaluated at the upstream dam face, a downstream displacement at the crown cantilever section thus means that the upstream face is pushed towards the rest of the dam, causing compressive stress at the dam face. Comparing the crown cantilever section displacement in figure 5.3b, also in figure 5.4b, and the minimal principal stress along the crown cantilever section in figure 5.4c, it is observed that the displacement and the minimal principal stress along the crown cantilever section show similar shapes in the lower part of the dam. Also, the maximal principal stress, in figure 5.4d, is negative in the majority of the crown cantilever section, meaning that there is no tensile stress, only compressive stress. The displacement of the crown cantilever section when only the self-weight load is applied is shown in figure 5.4a, in this case the displacement is mainly pointed towards the upstream face, or the empty water basin. This effect is noticed in the displacement of figure 5.4b, towards the top of the dam where the hydrostatic load becomes weaker, the self-weight load becomes dominant and the dam is displaced upstream. Also, at the top of the dam, the maximal principal stress becomes positive, meaning that there is tensile stress in the region. In summary, the compressive stress on the upstream face is caused by the downstream deformation that in itself is caused by the hydrostatic load. Furthermore, the downstream deformation is counteracted by the dam's own weight pushing it in the upstream direction.

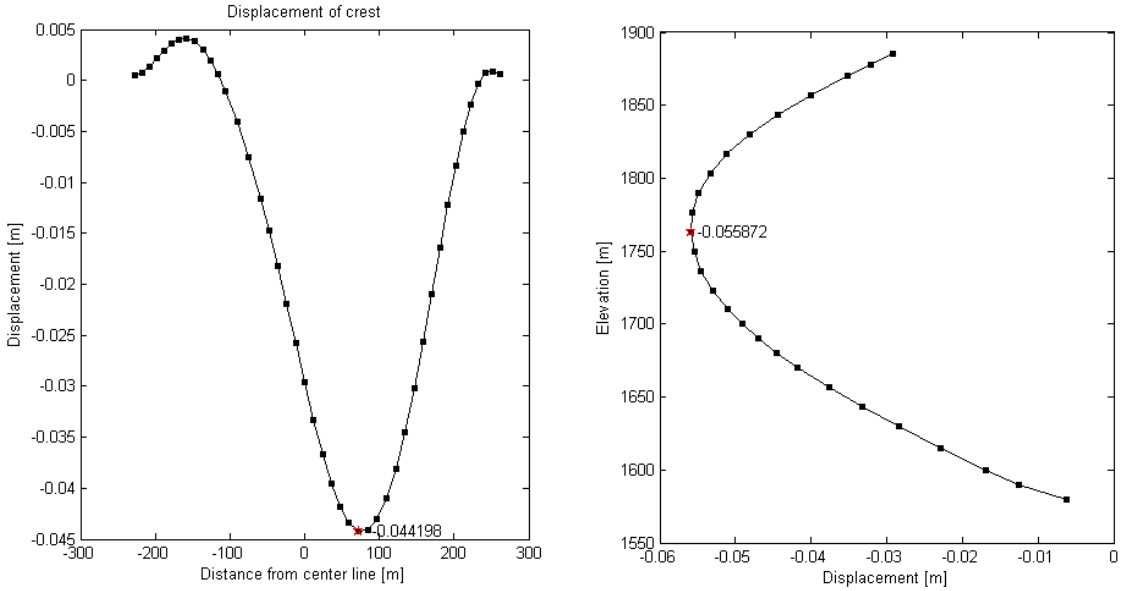

(a) *Crest line.* (b) *Crown cantilever section.*

Figure 5.3: *Displacement in CASE 1.*

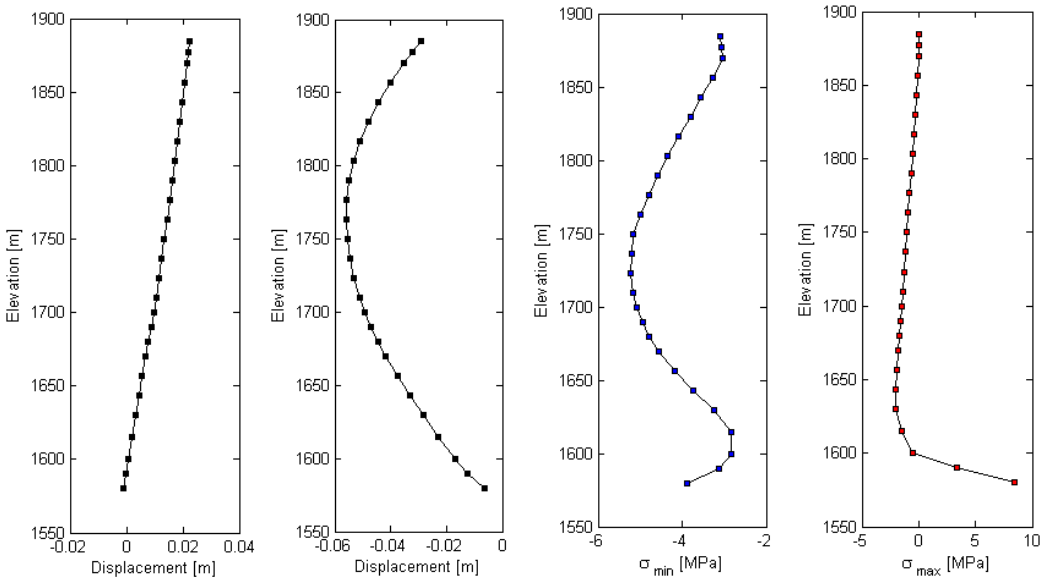

(a) (b) (c) (d)

Figure 5.4: *Displacement and principal stresses along the crown cantilever section for CASE 1. Figures (a) and (b) show the displacement of the crown cantilever section when only self-weight load is applied and for CASE 1, with all loads included. The minimal and maximal principal stress along the crown cantilever section in CASE 1 are illustrated in (c) and (d).*

5.1.2 CASE 2 - Normal water level, minimum temperature

The principal stresses, for CASE 2, at the upstream and downstream faces are shown in figures 5.5 and 5.6, respectively. The size of the extreme values are presented in table 5.1. The stress on the upstream dam face was slightly more negative in the minimum

temperature case compared to the case with maximum temperature, meaning that the dam is more compressed when the temperature is low. However, the principal stresses on the downstream surface are slightly more positive in CASE 2, meaning that the downstream surface is slightly less compressed. Lower temperatures reduces the volume of concrete. When the volume of the arch dam is reduced, the curvature of the arch decreases, flattening the dam. This decreases the upstream surface area, while the downstream surface area increases. This explains the more negative principal stresses on the upstream surface and the less negative stresses on the opposite side.

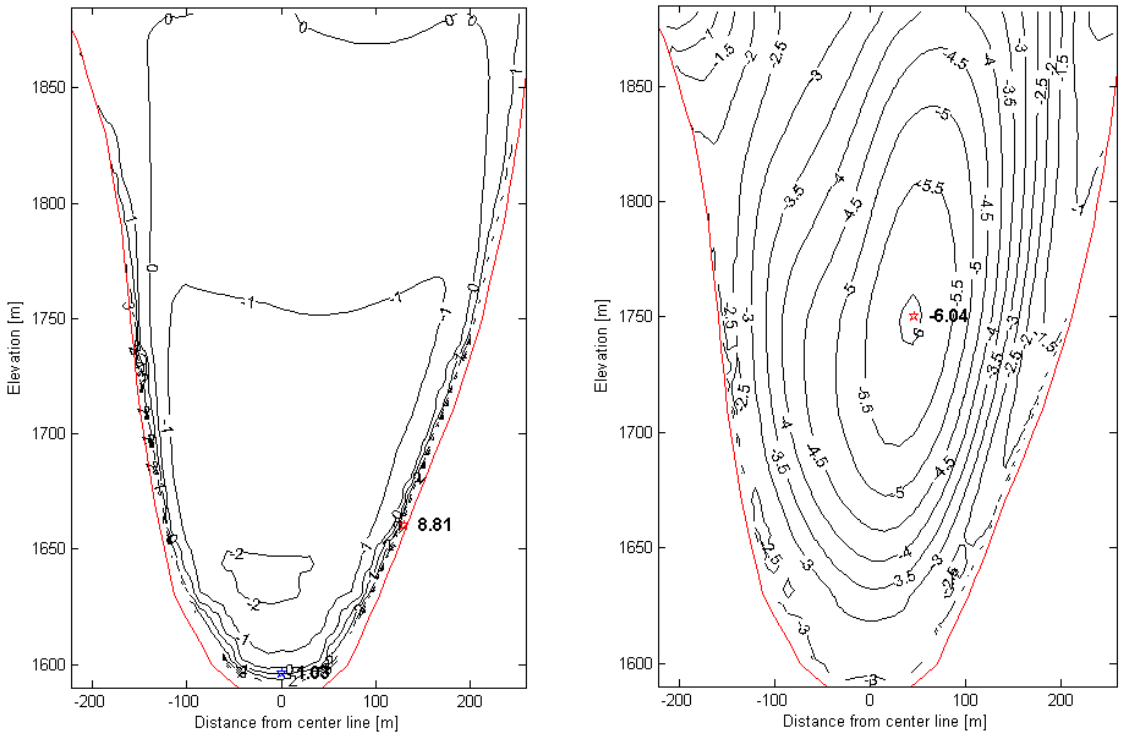

(a) *Maximal principal stress [Mpa].* (b) *Minimal principal stress [Mpa].*

Figure 5.5: *Principal stress at the upstream dam face in CASE 2. The stars denote extreme values.*

The result of the displacement can be seen in figure 5.7 and the extreme values are presented in table 5.3.

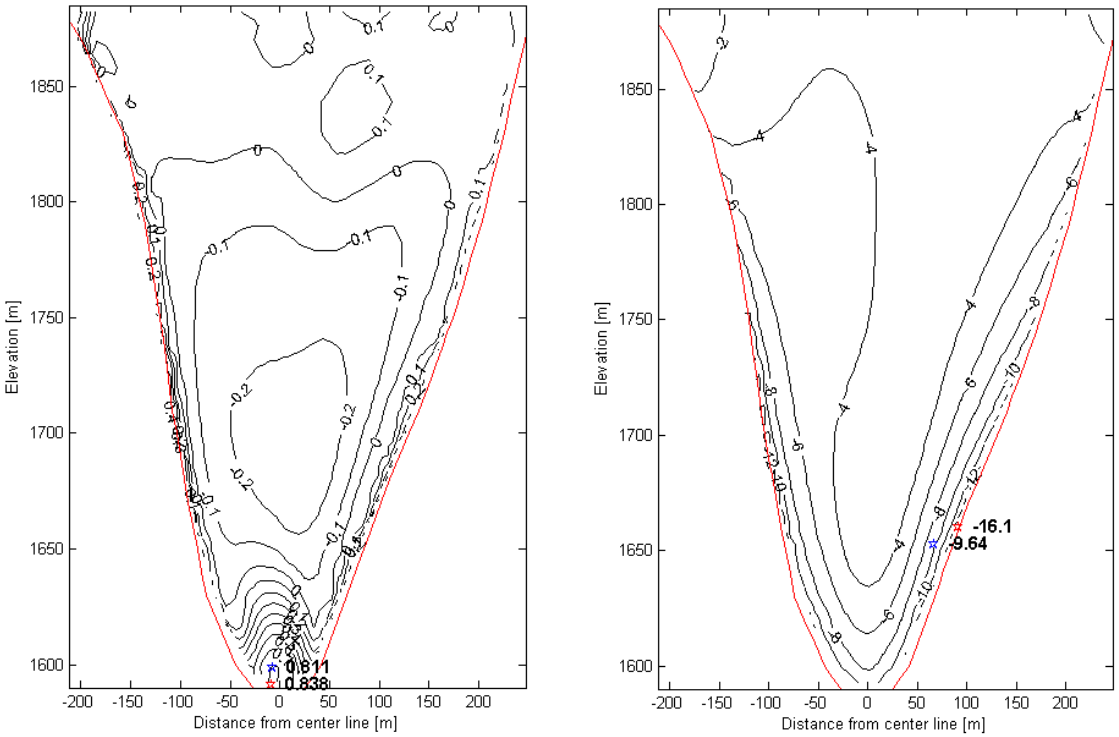

(a) *Maximal principal stress [Mpa].* (b) *Minimal principal stress [Mpa].*

Figure 5.6: *Principal stress at the downstream dam face in CASE 2. The stars denote extreme values.*

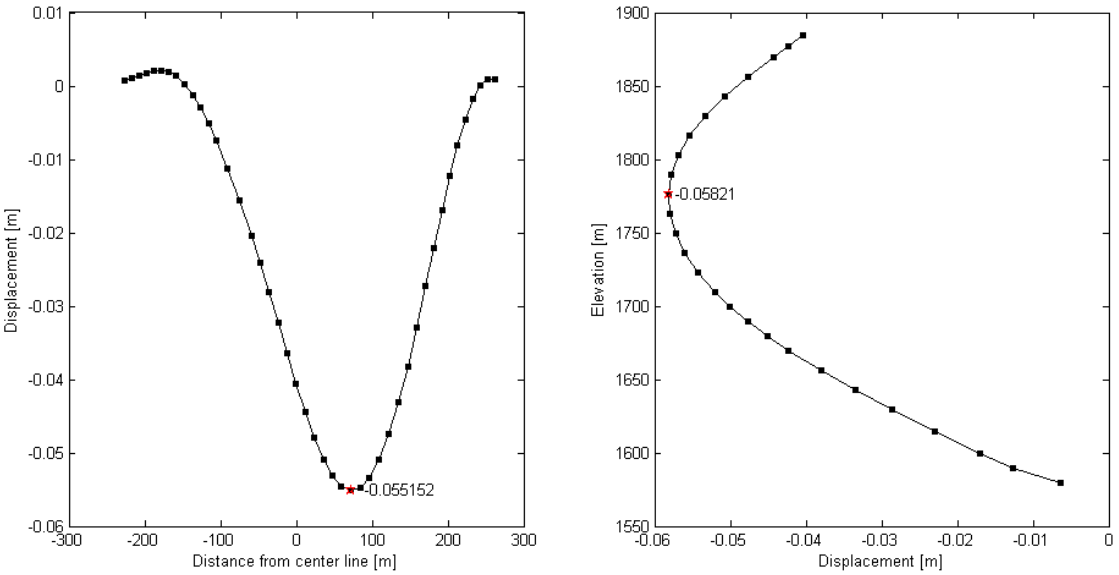

(a) *Crest line.* (b) *Crown cantilever section.*

Figure 5.7: *Displacement for CASE 2.*

5.1.3 CASE 3 - Dead water level, maximum temperature

The principal stresses on the upstream face, in CASE 3, are shown in figure 5.8 and the extreme values are presented in table 5.1. Extreme values for the principal stresses are both situated in the stress concentration region. The alternative extreme value for the maximal principal stress was located just outside the stress concentration region, as in CASE 1 with normal water level. The maximal principal stress distribution show similar patterns as in CASE 1, below the water surface at 1800 m. Above the water level, the stress increases faster, and is thus larger, towards the edges. The alternative extreme value for the minimal principal stress was found in the lower middle of the dam. The minimal principal stress distributions for CASE 3 and 1 show different patterns, the stresses have smaller magnitude and the large stresses are concentrated at the lower part of the dam in CASE 3. The smaller extreme values are the result of a smaller water pressure due to the lower water level.

The result was compared to the result from the Ertan dam, illustrated in figure B.3, and it was found that the stress distributions correspond well. However, the extreme values differ in magnitude, and also in location for the maximal principal stress. At the upper edges there are regions where the stress exceeds the tensile strength of concrete of 1.2 MPa. Since these regions reach relatively far from the edges it can not be ruled out that these stresses are not caused by stress concentration.

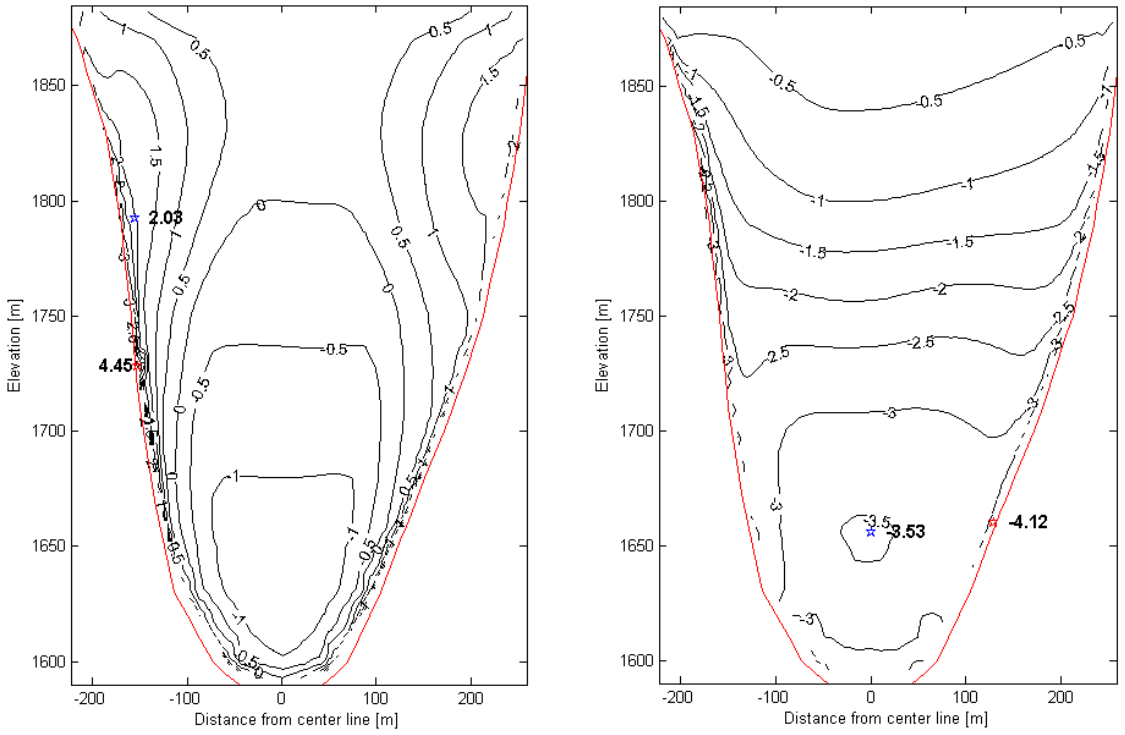

(a) *Maximal principal stress [Mpa].* (b) *Minimal principal stress [Mpa].*

Figure 5.8: *Principal stress at the upstream dam face CASE 3. The stars denote extreme values.*

The principal stresses at the downstream face is shown in figure 5.9 and the extreme values in table 5.1. The maximal principal stress was largest at the upper part of the dam, in contrast to CASE 1 where the largest maximal principal stress was found in the lower part

of the dam. For the minimal principal stresses the contours were similar for CASE 3 and 1 but with smaller magnitude in CASE 3.

A comparison of the result from the Ertan dam, illustrated in figure B.4, indicates that the distribution of the principal stresses correspond very well. The extreme values for the Jinping I dam have slightly larger magnitude and the maximum maximal principal stress exceeds the tensile strength of concrete.

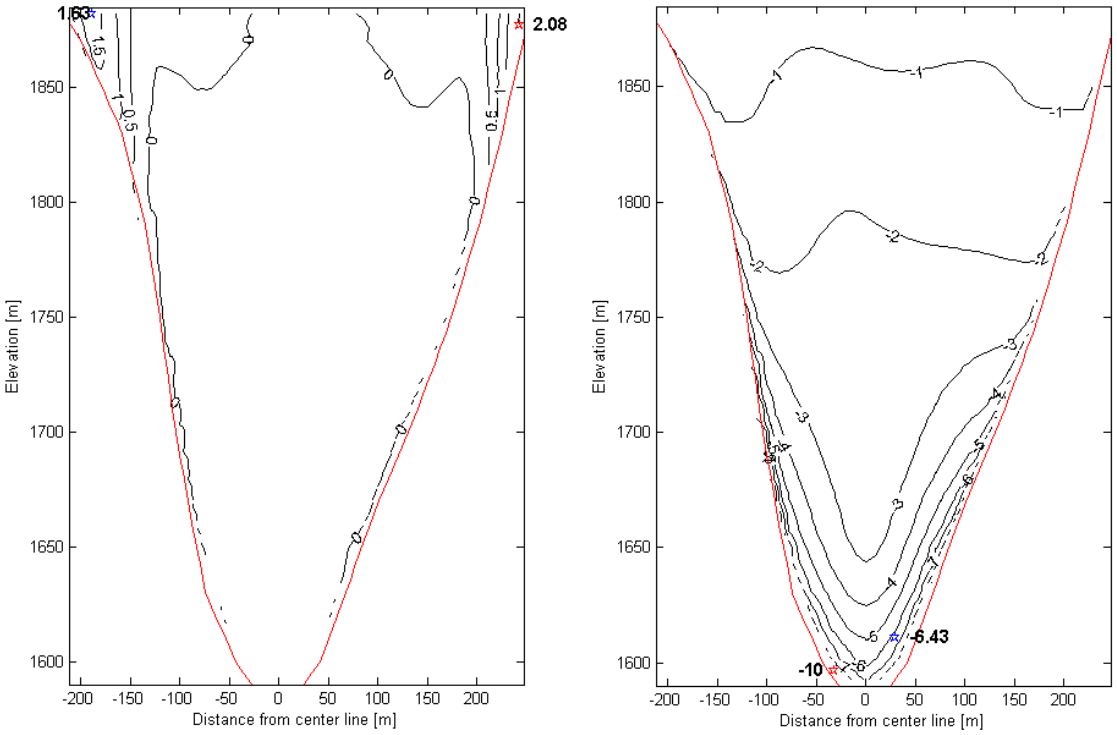

(a) *Maximal principal stress [Mpa].* (b) *Minimal principal stress [Mpa].*

Figure 5.9: *Principal stress at the downstream dam face in CASE 3. The stars denote extreme values.*

As can be seen in figure 5.10a the displacement of the crest line for CASE 3 was much smaller and in opposite direction, i.e. upstream, compared to CASE 1, presented in figure 5.3a. This was expected since the hydrostatic pressure downstream is decreased while the weight of the dam is constant, pushing the dam upstream. The same pattern was observed in the displacement of the crown cantilever section, seen in figure 5.10b, as compared to CASE 1 in figure 5.3b. In CASE 1 the displacement was directed downstream along the whole crown cantilever section, while the displacement in CASE 3 was directed upstream for heights above the dead water level at 1800 m.

As for CASE 1, the crown cantilever section displacement, figure 5.10b, also in figure 5.11a, was compared to the minimal principal stress on the upstream dam, figure 5.11b. Below the water level, at 1 800 m, the displacement and the stress at the crown cantilever section show approximately similar shapes. Above the water level, where the displacement becomes positive, the minimal principal stress is still negative indicating compression, although the compression is remarkably smaller than for CASE 1. Although, the maximal

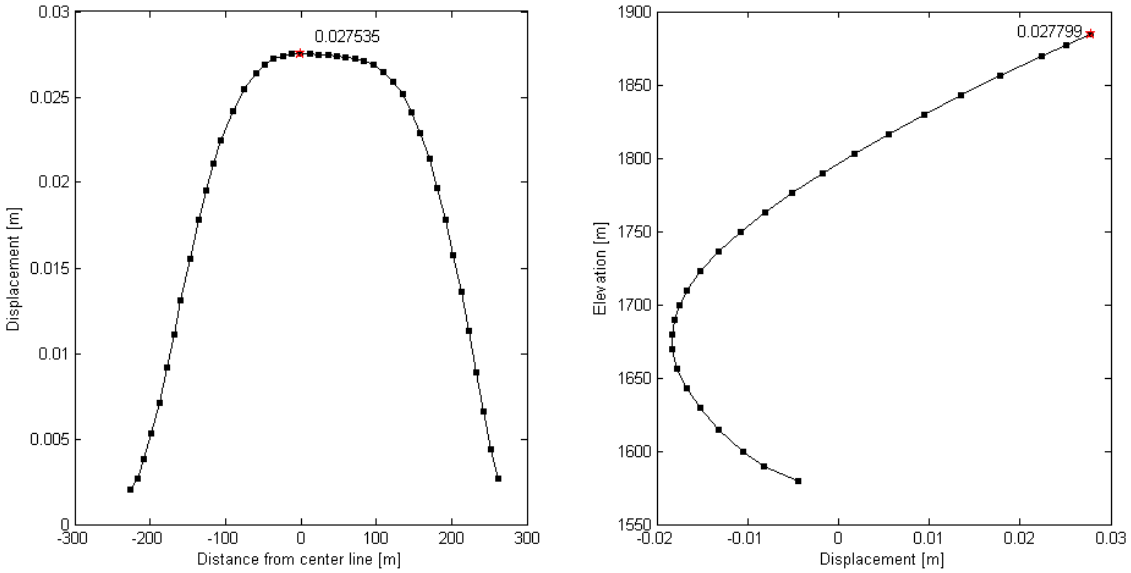

(a) *Crest line.* (b) *Crown cantilever section.*

Figure 5.10: *Displacement for CASE 3.*

principal stress, figure 5.11c, becomes positive above the water level. Thus, above the water level, both compressive and tensile stress occurs.

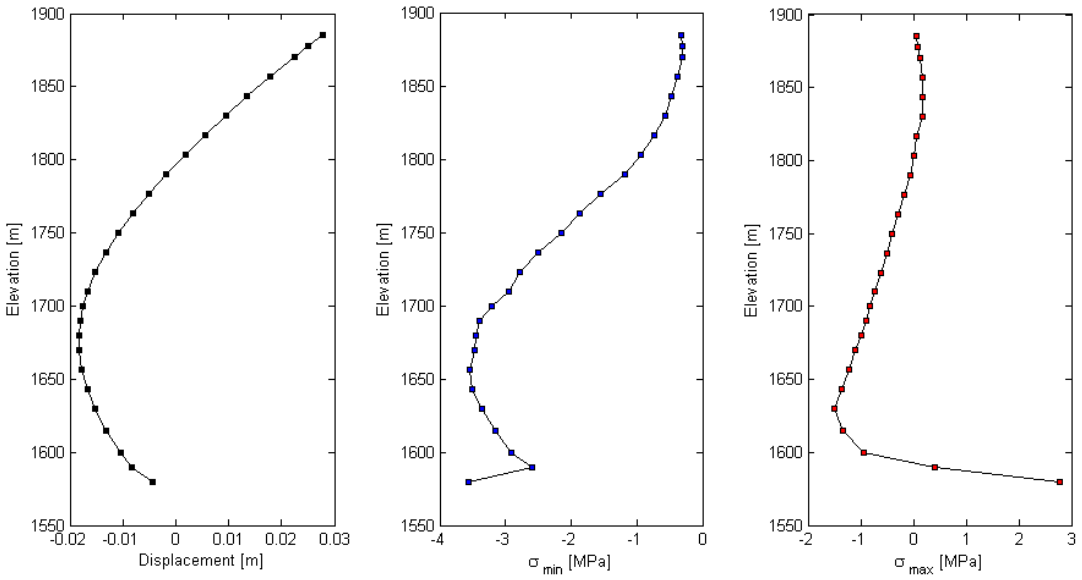

(a) *Displacement along the crown cantilever section.* (b) *Minimal principal stress.* (c) *Maximal principal stress.*

Figure 5.11: *Displacement and principal stresses along the crown cantilever section for CASE 3.*

5.1.4 CASE 4 - Dead water level, minimum temperature

The results for the stress and displacement in CASE 4, are presented in figures 5.12 to 5.14 and in tables 5.1 and 5.3. The minimum temperature load resulted in smaller maximal principal stresses and also slightly more negative minimal principal stresses on the upstream surface. On the downstream face the principal stresses were slightly more positive than in the maximum temperature case. This is caused by the reduced volume, as explained in section 5.1.2.

All contour plots of the Jinping I dam show similar stress distributions to those of the Ertan dam, illustrated in figure B.5 and B.6. The minimum values of the minimal principal stress on both the upstream and downstream face correspond well for the two dams. However, the maximum maximal principal stresses are larger for the Jinping I dam. The extreme value of the maximal principal stress exceeded the tensile strength of concrete on both the upstream and downstream faces.

The displacements of the crest line and the crown cantilever section are found in figure 5.14, with extreme values in table 5.3. The displacement plots show the same pattern as for CASE 3 with maximum temperature, with the crest line displacement directed upstream and the crown cantilever section displacement directed upstream for heights above the water level.

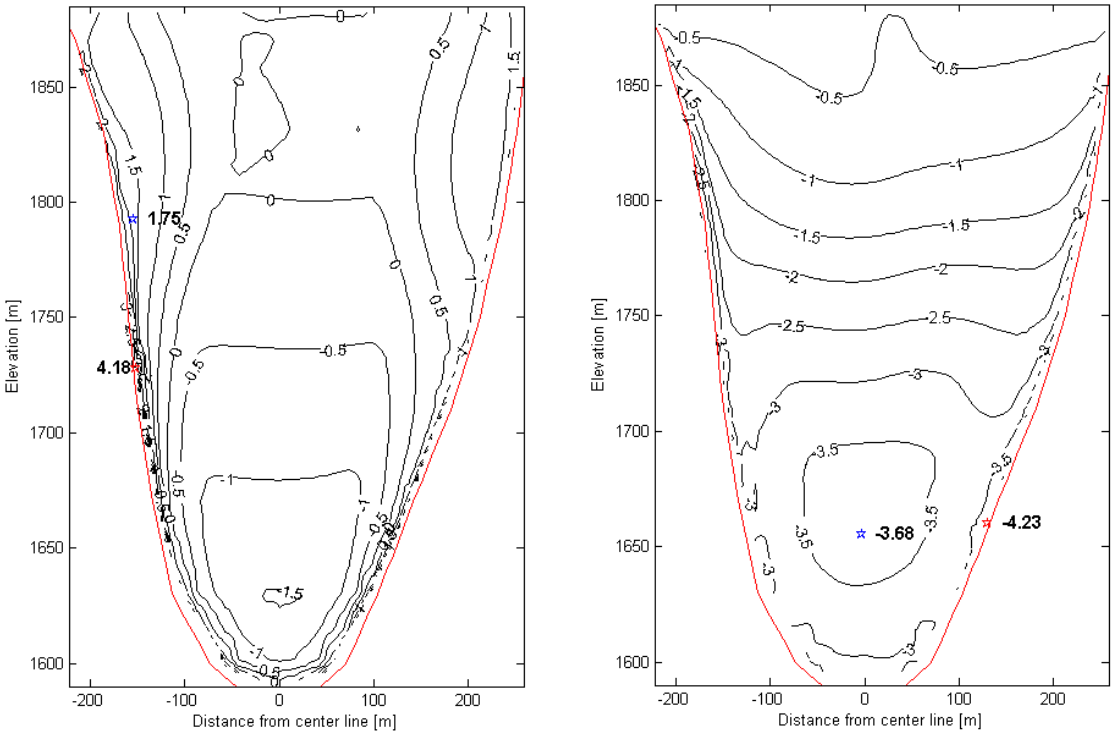

(a) *Maximal principal stress [Mpa].* (b) *Minimal principal stress [Mpa].*

Figure 5.12: *Principal stress at the upstream dam face in CASE 4. The stars denote extreme values.*

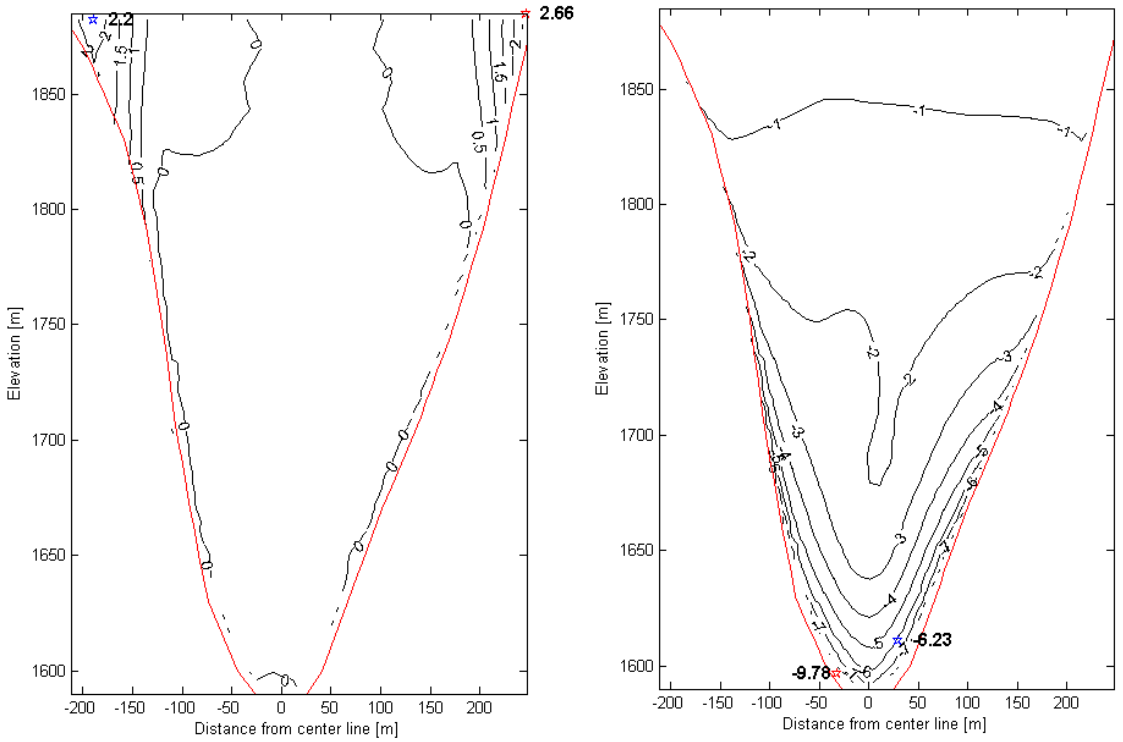

(a) *Maximal principal stress [Mpa].* (b) *Minimal principal stress [Mpa].*

Figure 5.13: *Principal stress at the downstream dam face in CASE 4. The stars denote extreme values.*

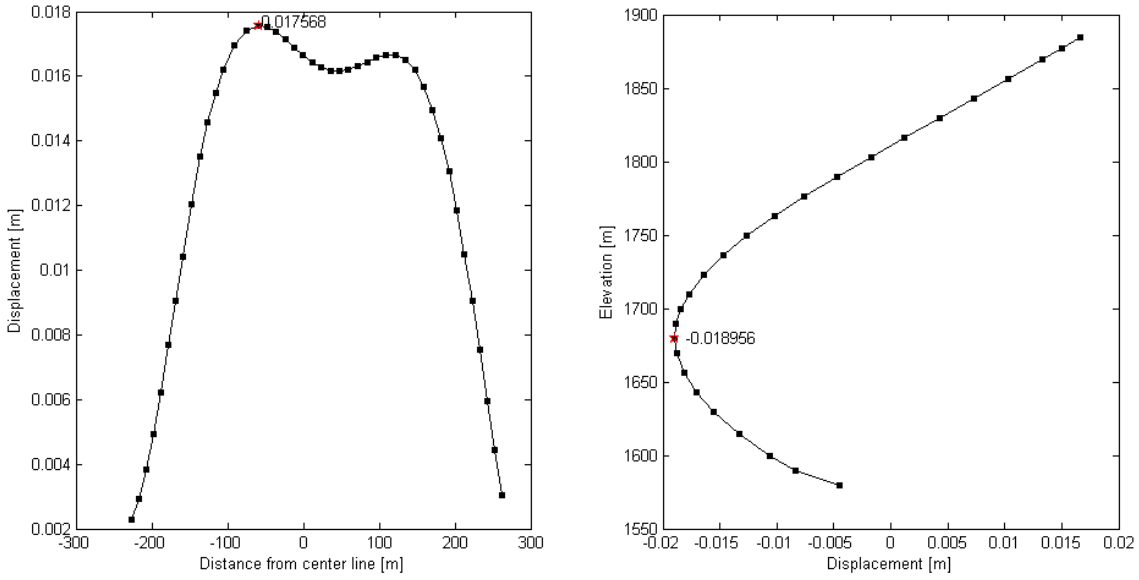

(a) *Crest line.* (b) *Crown cantilever section.*

Figure 5.14: *Displacement for CASE 4.*

5.1.5 CASE 5 - Design flood water level, maximum temperature

Principal stresses and deformations for CASE 5 are shown in figures 5.15 - 5.17. The extreme values for the stresses and the displacements are presented in table 5.1 and 5.3 respectively. As expected the results are very similar to the results for CASE 1 with normal water level, since the only difference in applied load is the water height which differs 0.26 m.

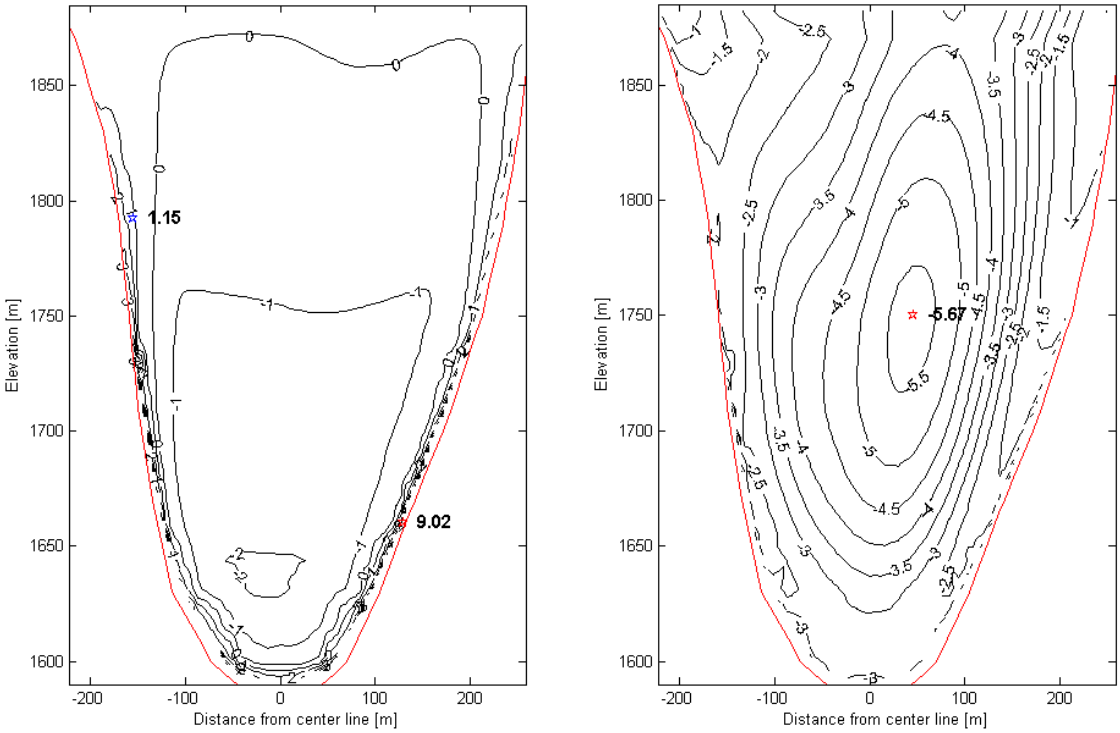

(a) *Maximal principal stress [Mpa].* (b) *Minimal principal stress [Mpa].*

Figure 5.15: *Principal stress at the upstream dam face in CASE 5. The stars denote extreme values.*

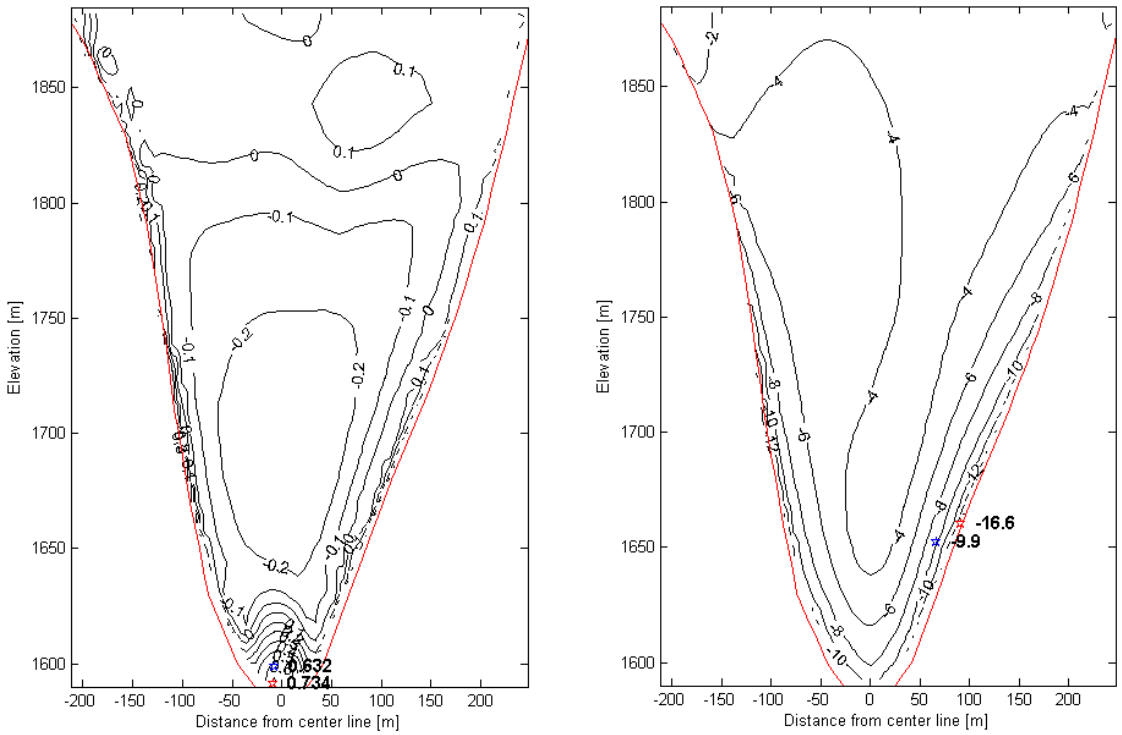

(a) *Maximal principal stress [Mpa].* (b) *Minimal principal stress [Mpa].*

Figure 5.16: *Principal stress at the downstream dam face in CASE 5. The stars denote extreme values.*

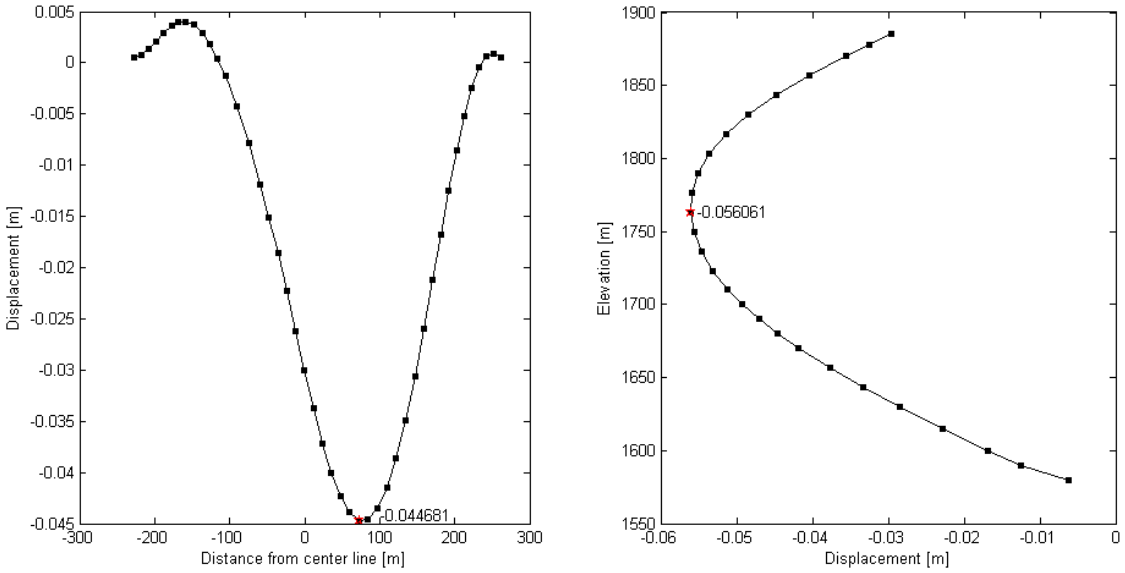

(a) *Crest line.* (b) *Crown cantilever section.*

Figure 5.17: *Displacement for CASE 5.*

5.1.6 CASE 6 - Check flood water level, maximum temperature

Figure 5.18 and 5.19 show the principal stresses, for CASE 6, of the upstream and downstream face, respectively. The stress distribution was similar to the stress distribution in

CASE 1, normal water level. Furthermore, the extreme values on the downstream face and the minimum of the minimal principal stress on the upstream face are similar to CASE 1, both in location and magnitude, while the secondary maximum maximal principal stress on the upstream surface is situated in the bottom part of the dam. The minimum minimal principal stress on the downstream face exceeded the strength of concrete at the edges of the dam. To get an idea of how far into the dam the compressive stresses exceeded the compressive strength of concrete the stress concentration region was increased. At a thickness of 7 % of the dam height no stresses outside the stress concentration area exceeded the compressive strength of concrete.

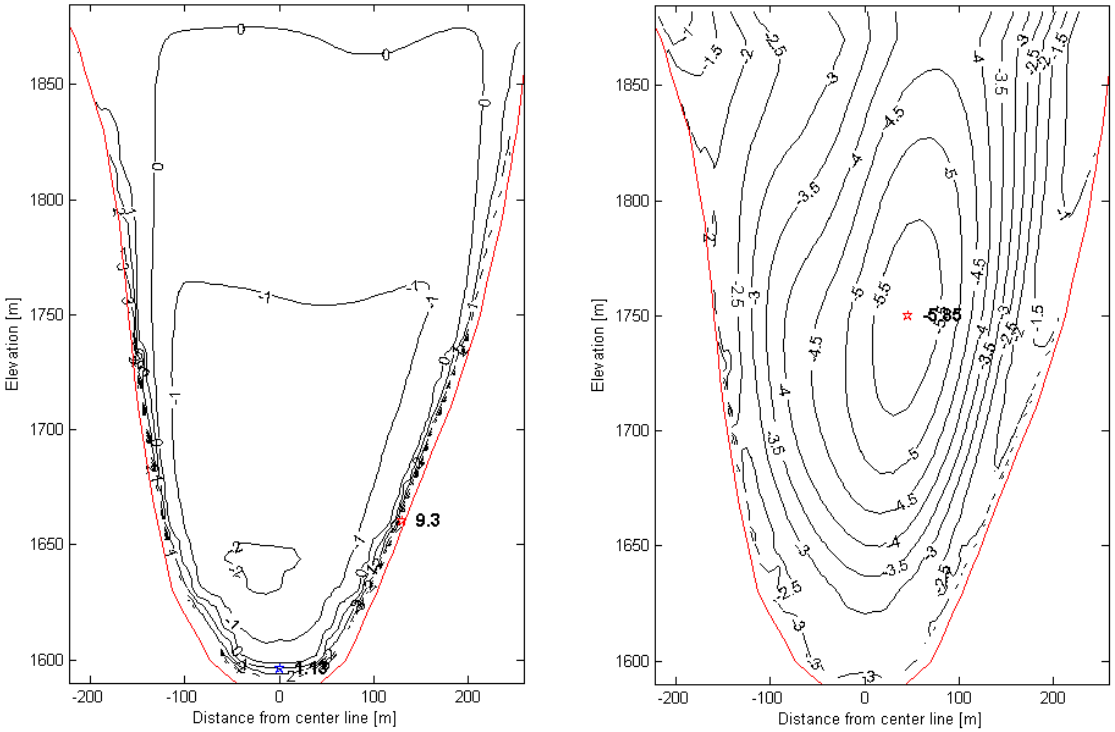

(a) *Maximal principal stress [Mpa].* (b) *Minimal principal stress [Mpa].*

Figure 5.18: *Principal stress at the upstream dam face in CASE 6. The stars denote extreme values.*

The displacement of the crest line and crown cantilever section can be seen in figure 5.20 with extreme values in table 5.3. The extreme values indicate that the largest displacement in the downstream direction, for the maximum temperature cases, will occur in CASE 6 which is expected since the hydrostatic load directed downstream is largest in this load case.

5.1.7 Summary of the static result.

From the results presented in section 5.1.1-5.1.6 it can be seen that the maximal principal stress at the upstream face have similar distributions for all load cases. The stress changes are steeper near the edges of the dam, where the maximum values were found.

The minimal principal stress at the upstream dam face had nearly the same stress dis-

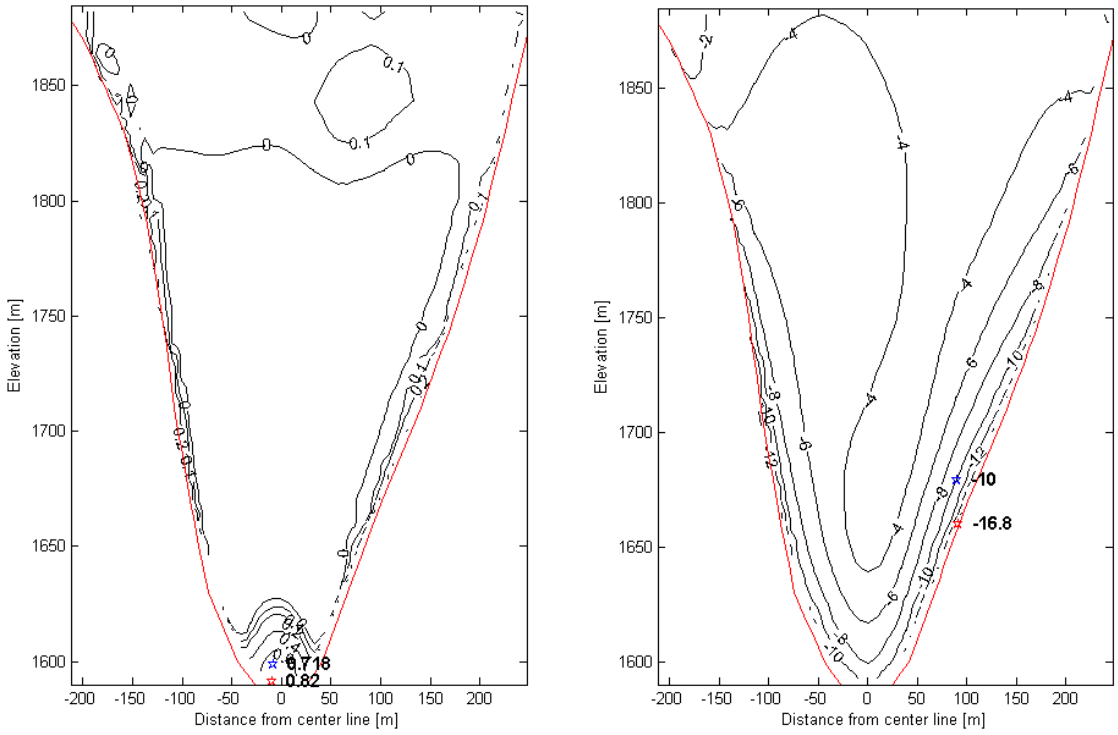

(a) *Maximal principal stress [Mpa].* (b) *Minimal principal stress [Mpa].*

Figure 5.19: *Principal stress at the downstream dam face in CASE 6. The stars denote extreme values.*

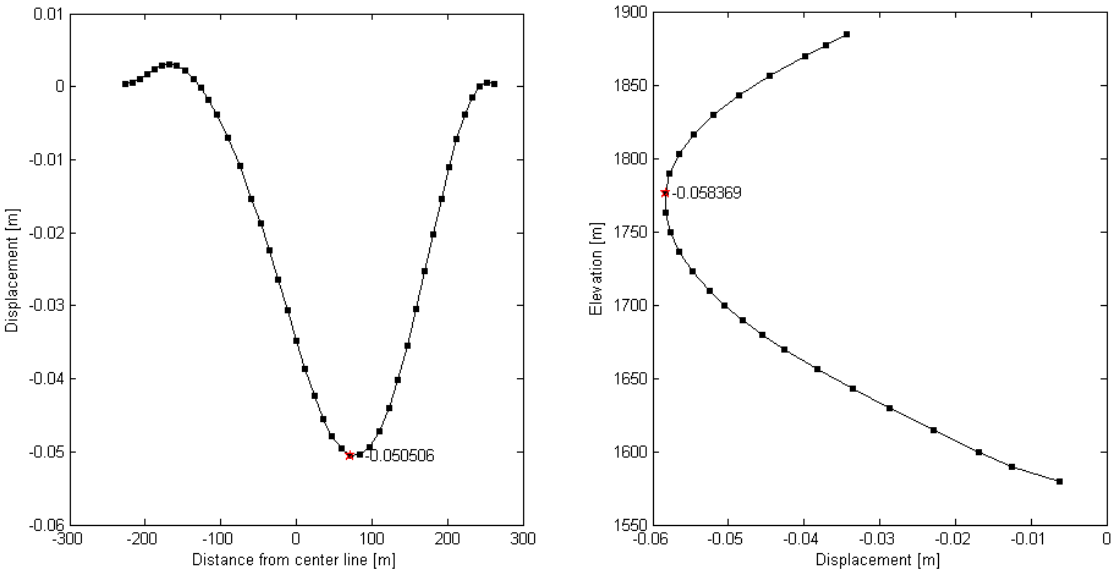

(a) *Crest line.* (b) *Crown cantilever section.*

Figure 5.20: *Displacement for CASE 6.*

tributions for CASE 1,2,5 and 6. The minimum stresses were found at the center of the

Table 5.1: *Extreme values of the principal stress for different load cases at the Jinping I dam. A * denotes extreme values due to stress concentration, a ** denotes the extreme value when the stress concentration areas have been removed.*

Load case	Maximal principal (MPa) Upface	Maximal principal (MPa) Downface	Minimal principal (MPa) Upface	Minimal principal (MPa) Downface
CASE 1	8.99*	0.732*	-5.66	-16.6*
	1.15**	0.629**		-9.88**
CASE 2	8.81*	0.838*	-6.04	-16.1*
	1.03**	0.811**		-9.64**
CASE 3	4.45*	2.08*	-4.12*	-10.0*
	2.03**	1.63	-3.53**	-6.43**
CASE 4	4.18*	2.66*	-4.23*	-9.78*
	1.75**	2.2	-3.68**	-6.23**
CASE 5	9.02*	0.734*	-5.67	-16.6*
	1.15**	0.632**		-9.9**
CASE 6	9.30*	0.820*	-5.85	-16.8*
	1.13**	0.718**		-10.0**

Table 5.2: *Extreme values of the principal stress for different load cases at the Ertan dam [21]. The load cases correspond to CASE 1, 3 and 4 for the Jinping I dam. A * denotes extreme values due to stress concentration and a ** denotes the extreme value when the stress concentration areas have been removed.*

Load case	Maximal principal (MPa) Upface	Maximal principal (MPa) Downface	Minimal principal (MPa) Upface	Minimal principal (MPa) Downface
Normal water level,	16.18*	0.47*	-5.67	-15.50*
maximal temperature	2.0**	0.10**		-8.0**
Dead water level,	8.78*	0.55*	-6.82*	-10.00*
maximal temperature	1.0**	0.41**	-3.46**	-6.0**
Dead water level,	9.01*	0.53*	-7.02*	-9.67*
minimal temperature	1.0**	0.48**	-3.50**	-6.0**

dam and the contour lines form an elliptical pattern with the stresses decreasing towards the edges. In CASE 3 and 4 the contour plots had similar elliptical patterns in the lower part of the dam, below the water level. In these load cases the minimum values were found at the edges of the dam, with an alternative minimum in the lower middle of the dam.

At the downstream face the maximal principal stress distributions form similar contour plots for CASE 1,2,5 and 6. Both the maximum and the second maximum values for the different load cases are smaller compared to the values at the upstream face and located at the bottom of the dam. For CASE 3 and 4 the maximal principal stress distributions were negative and close to zero in the major part of the dam and grew larger at the upper corners.

At the downstream face the distribution of the minimal principal stress had similar shapes for CASE 1,2,5 and 6. The minimum and the second minimum values of these cases were all situated at similar position, at the right side of the edge, and were also very large. For CASE 3 and 4 the extreme and the second extreme values were somewhat smaller than the extreme values of the other cases, and are situated at the bottom of the dam.

In load cases where stress results from the Ertan dam were available the Jinping results were verified and it was found that the stress distributions correspond well for the majority

Table 5.3: *Extreme values of the displacement for different load cases at the Jinping I dam.*

	Displacement (mm)	
Load case	crest line	Crown cantilever section
CASE 1	-44.2	-55.9
CASE 2	-55.2	-58.2
CASE 3	27.5	27.8
CASE 4	17.6	-19.0
CASE 5	-44.7	-56.1
CASE 6	-50.5	-58.4

of the load cases. The comparison of the extreme values for the two dams showed slight differences in magnitude. Furthermore, comparison of the extreme values and the strength of concrete indicated that the extreme values will exceed the allowed values in some cases.

The deformation of the dam was evaluated at the crest line and the crown cantilever section of the dam. CASE 1,2,5 and 6 showed nearly the same displacement curves of the crest line and crown cantilever section, with negative values indicating displacement in the downstream direction. The displacement of the crest line was largest in the center of the dam and the largest displacement magnitude was reached about 100 m to the right of the crown cantilever section. For the crown cantilever section the displacement was largest at the upper part of the dam with extreme values located between 1 750 and 1 800 m for CASE 1,2,5 and 6. At maximum temperature, CASE 6 contributes to the largest displacement of both the crest line and the crown cantilever section.

In CASE 3 and 4 the displacement of the crest line was positive, indicating displacement in the upstream direction. Furthermore the extreme values of the crest line displacement was reached to the left of the crown cantilever section. The displacements of the crown cantilever section at the dead water level cases were also affected by the decreased water level. The displacement below the water level was directed downstream, and above water level it was directed upstream, indicating that the self-weight load pushes the dam upstream when the hydrostatic pressure is removed. The extreme values were found at different locations for maximum and minimum temperatures. Both cases have a local minima around the height 1 700 m, where the extreme value for the minimum temperature is found. The largest displacement for the maximum temperature is found at the top of the dam in the upstream direction.

5.2 Dynamic conditions

The extreme values over the whole time span of the principal stresses for each node on the upstream face are displayed in figure 5.21. Indicated in the subfigures are also the most extreme stresses of the dam face and their position. The maximal principal stresses are shown in figure 5.21a. Just as in the static conditions in CASE 1, there were regions of negative stress, meaning that only compression occurs. Excluding areas of stress concentration, the extreme values of both the maximal and minimal principal stress are situated in the top middle of the dam, meaning that the dam is both most compressed and most tense in this area. As will be shown shortly, the dam also had the largest displacements in this area.

The stress distributions on the upstream face of the Jinping I dam, figure 5.21, can be compared to the stress distributions of the Ertan dam under a dynamic load of equal prob-

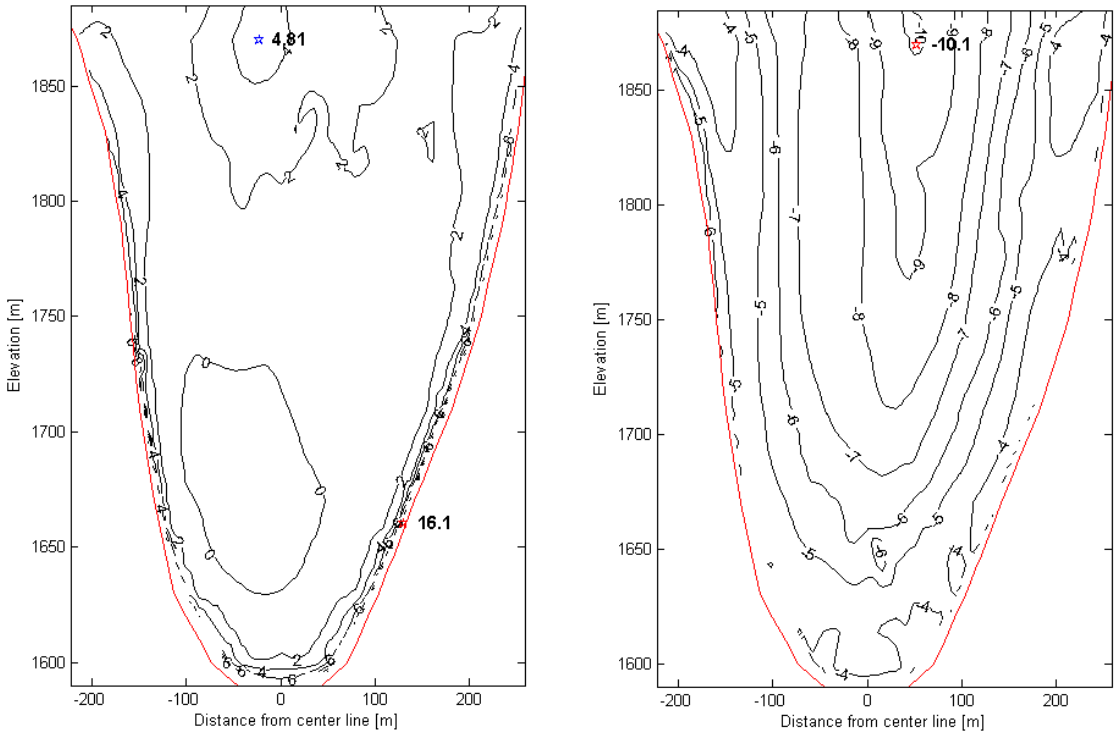

(a) *Maximum values of the maximal principal stress.* (b) *Mimimum values of the minimal principal stress.*

Figure 5.21: *Extreme values of the principal stresses for each node on the upstream face. The stars denote extreme values.*

ability in figure B.7. The extreme values of the principal stresses for both dams are found in table 5.4. The maximum maximal principal stresses of figure 5.21a correspond very well to the stress distribution of the Ertan dam, illustrated in figure B.7a, both dam faces have a local maxima in the upper middle part. The Ertan dam does not appear to indicate any negative stresses as a maximum maximal principal stress in any node. The distribution of minimum minimal principal stress of the Jinping I dam in figure 5.21b, is also very similar to the stress distribution of the Ertan dam, figure B.7b, with values closer to zero near the edges and reaching a minimum value at the top middle of the dam face.

Table 5.4: *Extreme values of the principal stress for the whole time span of the Jinping I and Ertan dams [21] in the dynamic load case. A * denotes extreme values due to stress concentration and a ** denotes the extreme value when the stress concentration areas have been removed.*

Dam	Maximal principal (MPa)		Minimal principal (MPa)	
	Upface	Downface	Upface	Downface
Jinping I	16.1* 4.81**	4.23	-10.1	-21.6* -13.7**
Ertan	21.78* 4.49**	4.69	-11.01	-15.69* -11.25**

The extreme values of the principal stresses for each node on the downstream face are dis-

played in figure 5.22. Indicated in the figures are also the position and value of the most extreme stresses, including and excluding stress concentration regions. The maximal principal stress shown in figure 5.22a shows regions of negative values, where there is constant compression. In the upper part of the dam the maximum stress values are larger, a large region experiences stresses that are larger than the tensile strength of concrete. Figure 5.22b shows the nodal minimum of minimal principal stress. The minimum value of -13.7 MPa is nearly 1.5 times the compressive strength of concrete. Even though this specific value is close to the region of stress concentration and it can be suspected that stress concentration contributes to its large magnitude, there are large parts of the dam experiencing stresses with a larger magnitude than the compressive strength of concrete.

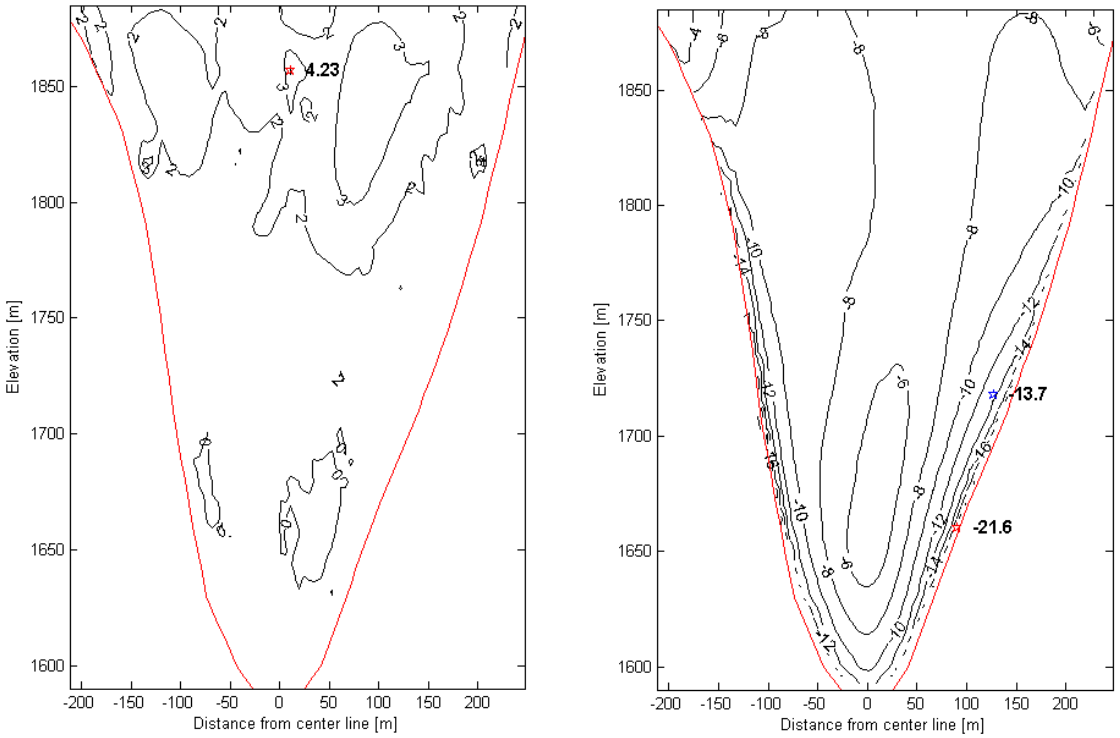

(a) *Maximum values of the maximal principal stress.* (b) *Mimimum values of the minimal principal stress.*

Figure 5.22: *Extreme values of the principal stresses for each node on the downstream face. The stars denote extreme values.*

The stress distributions on the downstream face of the Jinping I dam, figure 5.22, can be compared to stress distributions of the Ertan dam under similar dynamic conditions, shown in figure B.8, and the extreme values of the principal stresses for both dams are found in table 5.4. The distribution of maximal principal stresses of the two dams show evident similarities, although the Ertan dam does not indicate negative values for the maximum values of the maximal principal stress. The maximum stress value of the Jinping I dam was situated in the same region as the maximum stress value of the Ertan dam, in the top middle of the dam face, and the two maximum values were approximately of the same magnitude, 4.23 MPa for the Jinping I dam and 4.69 MPa for the Ertan dam. The distribution of nodal minima of minimal principal stress of the Jinping I dam, figure 5.22b, shows some similarities to the stress distribution of the Ertan dam, figure B.8b, with larger stress

magnitudes on the lower edges of the dams and decreasing magnitudes towards the lower middle of the dam face. Although, for the Jinping I dam, the extreme value found was of larger magnitude.

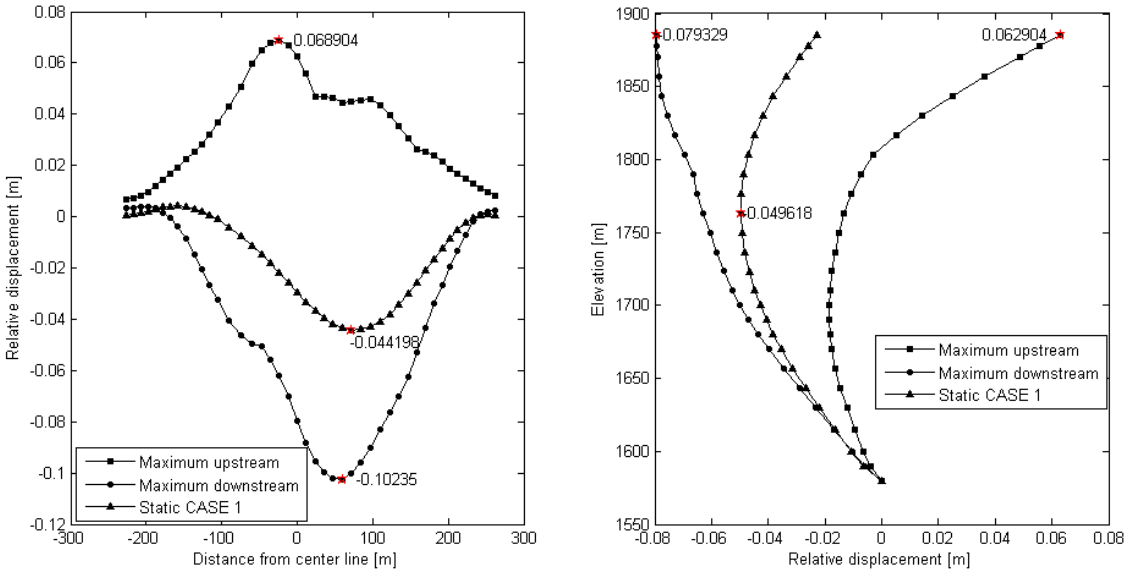

(a) *Crest line.* (b) *Crown cantilever section.*

Figure 5.23: *Maximum displacement upstream and downstream of each node on the crest line and crown cantilever section.*

Figure 5.23 shows the maximum upstream and downstream displacement of each node on the crest line and crown cantilever section, relative to the upstream bottom node. Included in the figure is also the displacement of CASE 1, for comparison. The downstream displacement of the crest line under dynamic load, in figure 5.23a, somewhat resembles the displacement in CASE 1 where the dam is only subjected to static load. The maximum displacements were situated in the same region, with the dynamic maximum at $x = 59.3\,\mathrm{m}$ and the static maximum at $x = 71.9\,\mathrm{m}$. As expected, the displacement magnitudes were larger in the dynamic case. The displacement of the crest line was larger in the downstream direction, which is expected since the static load directs the dam crest in this direction. The downstream maximum displacement of the crown cantilever section under dynamic load, figure 5.23b, can also be compared to its static counterpart. In the lower part of the dam both displacements point downstream, but around $z = 1750\,\mathrm{m}$, where the static displacement changes direction and starts to go upstream again, the dynamic maximum displacement continues to point downstream. This suggests that, in the lower part of the dam, the dam mainly moves upstream during dynamic load, while in the upper part, the dam moves both upstream and downstream. Figure 5.23b also shows an increasing distance between the maximum upstream and downstream displacements with increasing height, suggesting that the amplitude of the dam movement becomes larger with increasing height. Figure 5.24 shows the displacement of the top node and the middle node of the crown cantilever section as a function of time. The amplitude of the top node is of greater magnitude than for the middle node, this also suggests that the movement of the dam becomes larger in the upper part of the dam.

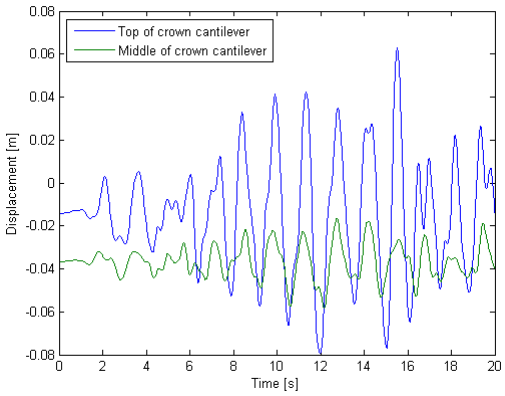

Figure 5.24: *Displacement of the top and middle node of the crown cantilever section as a function of time.*

Figure 5.25 shows the maximum downstream displacement of each node on the upstream face of the dam. The closer to the edges of the dam, where the dam is anchored to the foundation, the smaller the deformations. The maximum displacement has a magnitude of 10.2 cm and was found at the middle part of the crest line. The same displacement plot, but for the Ertan dam, can be found in figure B.9. The maximum displacement of the Ertan dam has the same appearance, with smaller displacements near the edges and a maximum displacement of 10.83 cm situated at the middle of the dam crest [21].

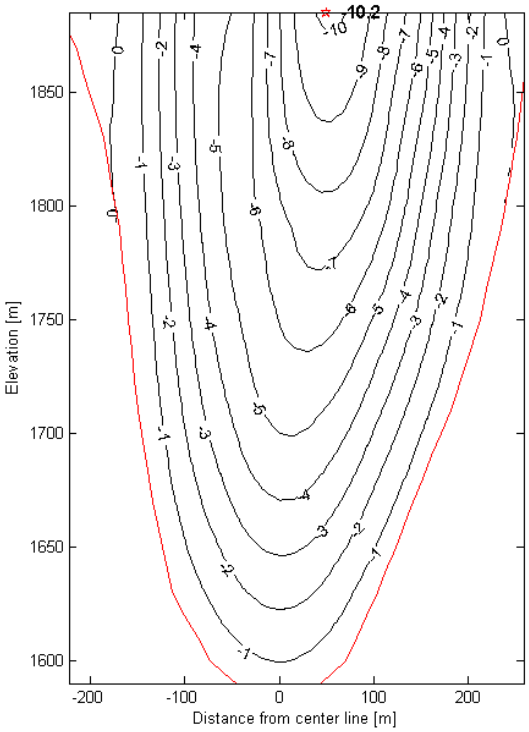

Figure 5.25: *Maximum downstream displacement of each node on the upstream face of the dam.*

Chapter 6:

Discussion

6.1 Static conditions

Due to the nature of the problem and the conditions the project were performed under, simplifications and assumptions had to be made. One obvious simplification when using FEM-calculations is that the material is assumed to consist of a finite number of interconnected nodes. The number of nodes affects the accuracy of the simulations and the computer power needed. More nodes does not always mean that the improved accuracy is worth the cost of more time-consuming simulations. A higher number of nodes could even worsen the problem of stress concentration. In this case it was not up to the authors to decide the number or distribution of nodes, since the model was made in advance.

The dam was assumed to consist of solid concrete, instead of concrete containing auxilliary structures. Such structures, as for example reinforcement bars or cavities, would locally change the elastic properties of the dam. But since reinforcements and other auxilliary structures constitute a relatively small portion of an arch dam, these deviations can be disregarded.

Another important assumption made was that both the rock and concrete behaved as linear elastic materials. An analysis assuming linear behaviour for all loads will not consider ruptures of the concrete. In this case, a non-linear analysis was beyond the scope of this project, and a linear analysis of another high arch dam was available for comparison of the results.

The FEM-simulations of the Jinping I dam in static conditions that could be compared with results of the Ertan dam under similar conditions, showed evident similarities, not only for extreme values of the principal stresses but also for the principal stress distribution. This confirms that the FEM-calculations performed on the Jinping I dam are accurate. Another way to verify the correctness of the calculations is to compare the load with the resulting displacements and stresses, and also compare how the displacements agree with the stresses. The principal stresses compared to the loads and displacements were studied at the crown cantilever section of the dam and showed expected results.

The stress distributions of the Ertan dam was not only used to validate whether the calculations were accurate, but also as a means to evaluate the safety of the Jinping I dam. One load case where the stress of the Jinping I dam differs from the stress of the Ertan dam is the dead water level case, where the tensile stresses in the upper corners of the dam are not only several times greater than the stresses in the Ertan dam, but also larger than the tensile strength of the concrete.

The safety of the dam was also verified by comparing the maximum and minimal stresses with the tensile and compressive strength of concrete. In CASE 3 and 4 there were tensile stresses found in the upper corners of the downstream face and upper edges of the upstream face that exceeded the tensile strength of concrete. The increased tensile stresses in these areas appears when the self-weight load is not counteracted by the hydrostatic load, and the dam crest is displaced upstream. To evaluate the formation and propagation of cracks in these areas a non-linear analysis is required. However, the position of critical stresses on the downstream face are favorable in the case of crack formation, since the site is relatively easy to access for restoration. The compressive strength of concrete was exceeded in CASE 1,2,5 and 6 in a small area near the right lower edge of the downstream face. When the stress concentration area was increased to 7 % of the dam height in CASE 6, where the largest compressive stresses were found, the maximum compressive stress was found to be smaller than the compressive strength of concrete. Thus, the area of unallowed stresses was found to be very small, and since it is situated near the stress concentration area, it is also suspected to be partly caused by stress concentration.

Evaluating whether stress in a certain region is caused by stress concentration or not is not an exact science when dealing with complex structures. Since it is not known how far from the dam-foundation interface stress concentration is an issue, there is no certain way of evaluating the extreme values of the stress. The method used when finding an extreme value not caused by stress concentration, as presented in table 5.1, was to find an extreme value when the stress concentration region, with a thickness of 5 % of the dam height, along the dam-foundation interface has been removed. As was discovered in the survey of stress concentrations in simple beams in section 3.2.1, a total of 10 % was needed to eliminate the regions of stress concentration. In the case of the Jinping I dam, an expansion of the eliminated area would in several cases lead to extreme values with smaller magnitudes.

6.2 Dynamic conditions

In addition to the assumptions and simplifications made for the static simulations, the dynamic simulations needed simplifications specific for dynamic conditions. The damping matrix was calculated according to the Rayleigh damping model, a common model used for concrete structures when specific data for the damping as a function of frequency is unavailable. The choice of damping ratio and modal frequencies will affect the damping and thereby the dynamic response of the dam.

Comparing the principal stresses of the dynamic case with the stresses of the static case, it is noticed that the magnitude of the stress increases all over both faces of the dam. However, the largest magnitude increase occurs in the upper part of the dam. This is expected since the time-dependent dam deformations are considerably larger in the upper parts of the dam.

The magnitudes of the principal stresses under dynamic load are in some areas considerably larger than the strength of concrete. However, due to the low probability of an earthquake, damages to the structure are allowed. Thus, it is more relevant to compare the stresses of the Jinping I dam to those of the Ertan dam, since the earthquake for each dam has equal probabilities. The principal stresses of the Jinping I dam are very similar to those of the Ertan dam, except for the minimal principal stress on the downstream face. The Jinping I dam has slightly larger compressive stress in areas around the lower sides of the dam, while the Ertan dam has a local maxima of compressive stress in the upper middle of the dam. However, measures of compressive stress is not of equal importance to

measures of tensile stress, since it is the tensile stress that causes cracking of concrete. Although the principal stress distribution of the Jinping I dam show large resemblance to the principal stress distribution of the Ertan dam, a non-linear analysis is needed to evaluate the behaviour of the concrete for stresses that exceeds the tensile strength.

Chapter 7:

Conclusion

The demand for electric power in China increases each year. Today, the majority of power is generated in coal-fired plants, contributing to large amounts of greenhouse gases and pollutants. Thus, it is of great importance that further development of power production focuses on clean power generation, where hydropower is a cheap and reliable alternative.

The static analysis showed that both tensile and compressive strength was exceeded in limited areas of the dam. The critical areas for the tensile stress are the upper corners of the downstream face and the upper edges of the upstream face. Critical tensile stresses only occured in CASE 3 and 4, which are the dead water level cases. The occurrence of dead water level is very unlikely, making the probability for critical tensile stresses caused by declined water level very low. However, there is a risk that the water drops to a level where the tensile stresses exceeds the tensile strength of concrete. To properly evaluate the risk of crack formation in the critical areas a non-linear analysis is needed. The critical areas for compressive stress are mainly situated at the lower edge of the downstream face. These areas are situated very close to stress concentration areas and can be suspected to be partly caused by stress concentration. Furthermore, the compressive stress is not the most important measure for structural safety.

The linear analysis of the dynamic case showed that the level of stresses in the dam are acceptable for an earthquake with this ground acceleration. However, to analyse cracking and crack propagation properly, a non-linear analysis is required.

Bibliography

[1] Wanga, Q., Chen, Y., (2009), Status and outlook of China's free-carbon electricity. *Renewable and Sustainable Energy Reviews.* 2010: 14, 1012-1025.
DOI: 10.1016/j.rser.2009.10.012

[2] Kahrl, F., et al., Challenges to China's transition to a low carbon electricity system. *Energy Policy.* (2011).
DOI: 10.1016/j.enpol.2011.01.031

[3] Huang, H., Yan, Z., (2008), Present situation and future prospect of hydropower in China. *Renewable and Sustainable Energy Reviews.* 2009: 13, 1652-1656.
DOI: 10.1016/j.rser.2008.08.013

[4] Shiyong, W., Manbin, S., Jian, W., (2010), Jinping hydropower project: main technical issues on engineering geology and rock mechanics. *Bulletin of Engineering Geology and the Environment.* 2010: 69, 325-332.
DOI 10.1007/s10064-010-0272-4

[5] Hydrochina chengdu engineering corporation (2010) *Jinping I Hydroelectric project.* Available at: <`http://chidi.com.cn/en/ShowNews.aspx?newsid=422`> [Accessed 30 Mars 2011]

[6] Novák, P., *Hydraulic Structures.* 3rd ed.[e-book], London: Spon Press
Available through: Tsinghua University Library website <`http://eng.lib.tsinghua.edu.cn/default.html`> [Accessed 14 April 2011]

[7] Vasiliev, V., Morozov, E., (2007), Chapter 1 -Introduction *Advanced mechanics of composite materials.* 2nd ed.[e-book], 1-30. Amsterdam, Boston, MA: Elsevier,
Available through: ScienceDirect <`http://www.sciencedirect.com/science/book/9780080453729`> [Accessed 14 April 2011]

[8] Silva, V., (2006), *Mechanics and strength of materials*[e-book], Berlin: Springer,
Available through: Springer <`http://www.springer.com/materials/mechanics/book/978-3-540-25131-6`> [Accessed 14 April 2011]

[9] Lundh, H., (2000) *Grundläggande hållfasthetslära*, Stockholm: Institutionen för hållfastighetslära, Kungliga tekniska högskolan.

[10] Rao, S.S.,(2005), 1 -Overview of Finite Element Method, *The Finite Element Method in Engineering.* 4th ed.[e-book], 3-49. Amsterdam, Boston, MA: Elsevier,
Available through: ScienceDirect <`http://www.sciencedirect.com/science/book/9780750678285`> [Accessed 14 April 2011]

[11] Patnaik, S., Hopkins, D.,(2004) Appendix 6 - Formulas of Strength of Materials *Strength of materials: A new unified theory for the 21st century* [e-book], 687-691.

Amsterdam, Boston, MA: Elsevier/Butterworth-Heinemann.
Available through: ScienceDirect <http://www.sciencedirect.com/science/book/9780750674027> [Accessed 25 Mars 2011]

[12] (1977), *Design Criteria for Concrete Arch and Gravity Dams*, Serie.19, United States Department of the interior, Bureau of Reclamation.
Available at: <http://www.usbr.gov/pmts/hydraulics_lab/pubs/EM/EM19.pdf> [Accessed 14 April 2011]

[13] Bao, T.F., Xu, B.S., Zheng, X.Q., (2011), Hybrid method of limit equilibrium and finite element internal force for analysis of arch dam stability against sliding. *Science China, Technological Sciences.* 2011: Vol.54, No.4, 793-798.
DOI: 10.1007/s11431-011-4312-5

[14] Clough, R. W., Penzien, J., (2003) *Dynamics of structures* 3rd ed., Berkeley, CA: Computers & Structures, Inc.

[15] Jennings, P. (2003). An introduction to the earthquake response of structures. In *International Handbook of Earthquake and Engineering Seismology*, William H.K. Lee, Hiroo Kanamori, Paul C. Jennings and Carl Kisslinger (ed.), 1097-1125. Boston: Academic Press
Available through: ScienceDirect <http://www.sciencedirect.com/science/issue/42575-2003-999189999.7997-666783> [Accessed 5 May 2011]

[16] Chopra, A. K., (2007) *Dynamics of structures: Theory and applications to earthquake engineering* 3rd ed., Upper Saddle River, N.J.: Pearson/Prentice Hall.

[17] US Army Corps Of Engineers, (2003), *Time-History Dynamic Analysis of Concrete Hydraulic Structures*, Manual No. 1110-2-6051, Washington, DC.
Available at: <http://140.194.76.129/publications/eng-manuals/> [Accessed 12 May 2011]

[18] US Army Corps Of Engineers, (2007), *Earthquake Design and Evaluation of Concrete Hydraulic Structures*, Manual No. 1110-2-6053, Washington, DC.
Available at: <http://140.194.76.129/publications/eng-manuals/> [Accessed 12 May 2011]

[19] Feng, J., Professor at Department of Hydraulic Engineering, Tsinghua University, Beijing, personal communication, March to May 2011.

[20] Gui, Y., PhD student at Department of Hydraulic Engineering, Tsinghua University, Beijing, personal communication, March to May 2011.

[21] Department of Hydraulic Engineering, (2009), *Seismic Analysis and Safety Evaluation of Arch dam in Ertan Hydropower Station*, Tsinghua University, Beijing. (Published in Chinese)

Appendices

Appendix A:

Temperature of the dam faces

Table A.1: *Difference between closure temperature and the maximum and minimum temperature during a year.*

	Maximum		Minimum	
Elevation (m)	T_m (°C)	T_d (°C)	T_m (°C)	T_d (°C)
1885	4.31	0.00	0.09	0.00
1870	2.22	3.68	0.07	0.54
1830	0.96	7.54	-.09	3.53
1790	0.48	8.06	-.30	4.39
1750	1.35	8.06	0.69	4.67
1710	1.29	8.04	0.71	4.76
1670	1.28	7.96	0.72	4.84
1630	1.04	7.20	0.65	5.00
1600	0.36	5.39	0.20	4.53
1580	-.10	4.20	-.10	4.20

Temperature of downstream and upstream dam face

$$T = T_m \pm \frac{T_d}{2}$$

Appendix B:

Stress and displacement of the Ertan dam

Static

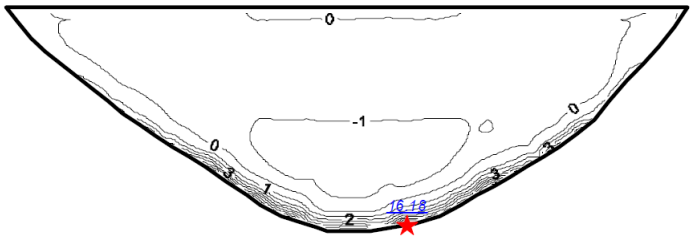

(a) *Maximal principal stress.*

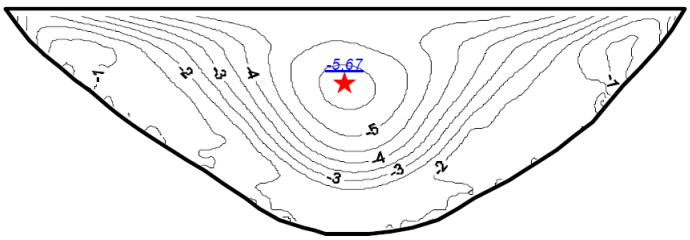

(b) *Minimal principal stress.*

Figure B.1: *Principal stresses at the upstream dam face of the Ertan dam at normal water level and maximum temperature. The stars indicate extreme values.*

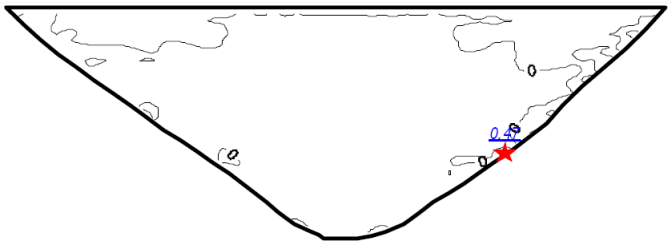

(a) *Maximal principal stress.*

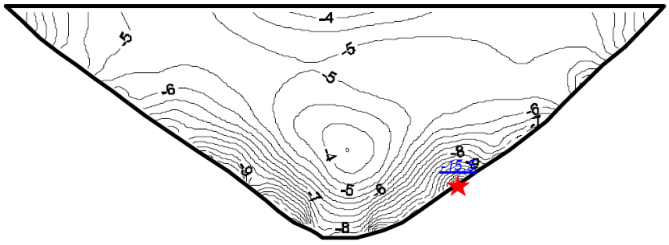

(b) *Minimal principal stress.*

Figure B.2: *Principal stresses at the downstream dam face of the Ertan dam at normal water level and maximum temperature. The stars indicate extreme values.*

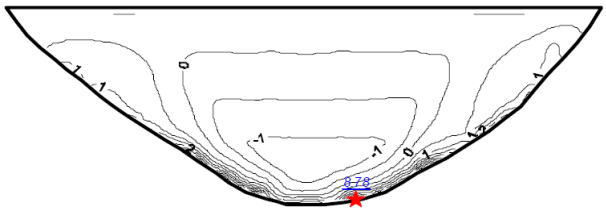

(a) *Maximal principal stress.*

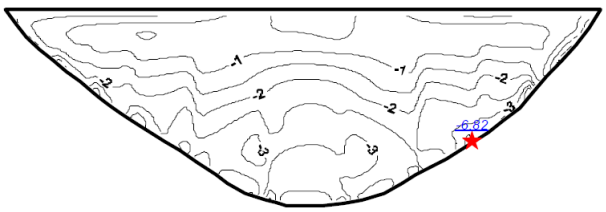

(b) *Minimal principal stress.*

Figure B.3: *Principal stresses at the upstream dam face of the Ertan dam at dead water level and maximum temperature. The stars indicate extreme values.*

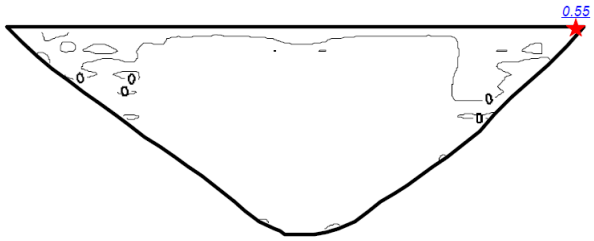

(a) *Maximal principal stress.*

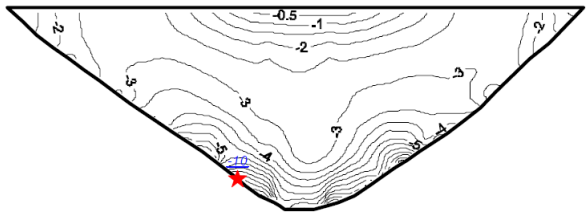

(b) *Minimal principal stress.*

Figure B.4: *Principal stresses at the downstream dam face of the Ertan dam at dead water level and maximum temperature. The stars indicate extreme values.*

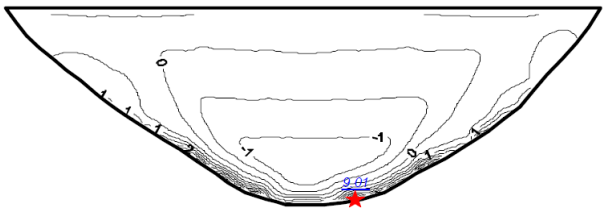

(a) *Maximal principal stress.*

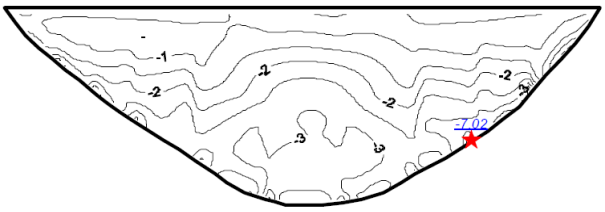

(b) *Minimal principal stress.*

Figure B.5: *Principal stresses at the upstream dam face of the Ertan dam at dead water level and minimum temperature. The stars indicate extreme values.*

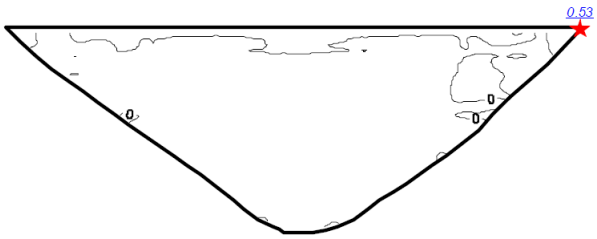

(a) *Maximal principal stress.*

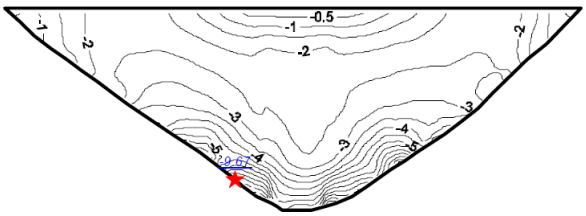

(b) *Minimal principal stress.*

Figure B.6: *Principal stresses at the downstream dam face of the Ertan dam at dead water level and minimum temperature. The stars indicate extreme values.*

Dynamic

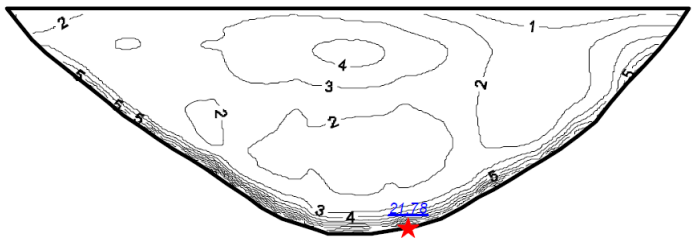

(a) *Nodal maximum of maximal principal stress.*

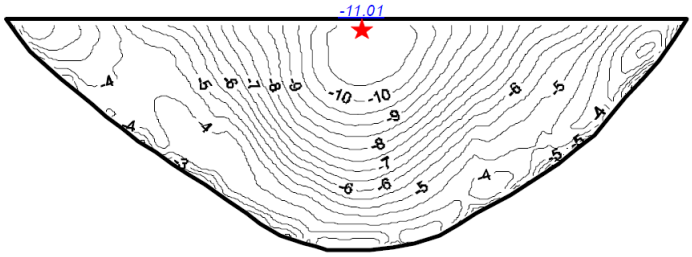

(b) *Nodal minimum of minimal principal stress.*

Figure B.7: *Nodal maximum and minimum of principal stresses at the upstream dam face of the Ertan dam under dynamic load. The stars indicate extreme values.*

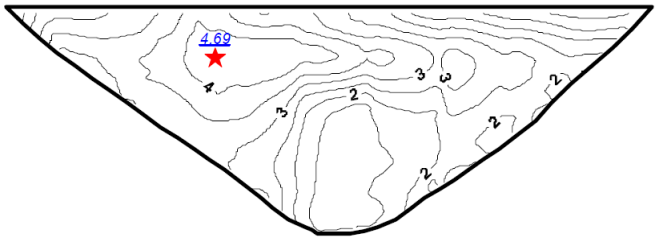

(a) *Nodal maximum of maximal principal stress.*

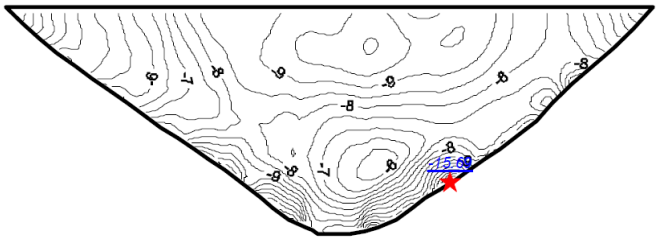

(b) *Nodal minimum of minimal principal stress.*

Figure B.8: *Nodal maximum and minimum of principal stresses at the downstream dam face of the Ertan dam under dynamic load. The stars indicate extreme values.*

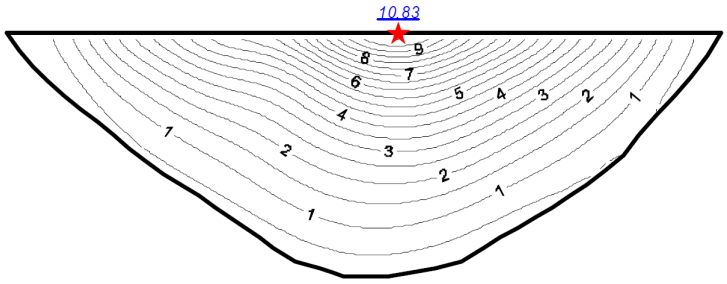

Figure B.9: *Displacement of the upstream face of the Ertan dam under dynamic load. The star indicates the maximum displacement [21].*